

Challenges and Strategies of Low-Pressure All-Solid-State Batteries

Jiaxu Zhang, Jiamin Fu, Pushun Lu, Guantai Hu, Shengjie Xia, Shutao Zhang, Ziqing Wang, Zhimin Zhou, Wenlin Yan, Wei Xia, Changhong Wang,* and Xueliang Sun*

All-solid-state batteries (ASSBs) are regarded as promising next-generation energy storage technology owing to their inherent safety and high theoretical energy density. However, achieving and maintaining solid–solid electronic and ionic contact in ASSBs generally requires high-pressure fabrication and high-pressure operation, posing substantial challenges for large-scale production and application. In recent years, significant efforts are made to address these pressure-related challenges. In this review, the impact of pressure on ASSBs is explored. First, the categories, origins, and challenges associated with pressure in ASSBs are outlined. Second, an overview of recent advancements in addressing pressure-related issues in ASSBs is provided, focusing on electrode materials and their interfaces with various solid-state electrolytes (SSEs). Third, advanced characterizations and simulations employed to unravel the intricate electrochemical–mechanical interactions in ASSBs are examined. Finally, existing strategies and the insights on achieving low-stack-pressure ASSBs are presented.

J. Zhang, P. Lu, G. Hu, S. Xia, S. Zhang, Z. Wang, Z. Zhou, W. Yan, W. Xia, C. Wang, X. Sun

Eastern Institute for Advanced Study

Eastern Institute of Technology

Ningbo 315200, China

E-mail: cwang@eitech.edu.cn; xsun@eitech.edu.cn

J. Zhang, P. Lu, G. Hu, W. Xia

School of Chemistry and Materials Science

University of Science and Technology of China

Hefei 230026, China

J. Zhang, P. Lu, G. Hu, C. Wang, X. Sun

Ningbo Key Laboratory of All-Solid-State Battery

Ningbo 315200, China

J. Fu

Department of Mechanical and Materials Engineering

University of Western Ontario

1151 Richmond St., London, Ontario N6A 3K7, Canada

 The ORCID identification number(s) for the author(s) of this article can be found under <https://doi.org/10.1002/adma.202413499>

© 2024 The Author(s). Advanced Materials published by Wiley-VCH GmbH. This is an open access article under the terms of the [Creative Commons Attribution-NonCommercial-NoDerivs](#) License, which permits use and distribution in any medium, provided the original work is properly cited, the use is non-commercial and no modifications or adaptations are made.

DOI: [10.1002/adma.202413499](https://doi.org/10.1002/adma.202413499)

1. Introduction

The quest for safer, more efficient, and high-performance energy storage solutions has led to significant advancements in battery technology. Among these, all-solid-state batteries (ASSBs) have emerged as a promising alternative to conventional liquid electrolyte batteries due to their potential for higher energy densities, improved safety, and longer cycle life.^[1,2] In this context, numerous solid-state electrolytes (SSEs) have been developed, including oxides,^[3] sulfides,^[4] halides,^[5] polymers,^[6] and oxychlorides.^[7] Some of these SSEs exhibit room-temperature ionic conductivities surpassing those of commercial liquid electrolytes,^[8,9] such as high-entropy SSEs ($\text{Li}_{9.54}[\text{Si}_{0.6}\text{Ge}_{0.4}]_{1.74}\text{P}_{1.44}\text{S}_{11.1}\text{Br}_{0.3}\text{O}_{0.6}$, 32 mS cm^{-1}).^[10] With significant advancements in SSEs, ASSBs exhibit remarkable electrochemical performance,

including high power density, extended cycle life, and excellent capacity retention at low temperatures.

Despite these advancements, ASSBs currently require high fabrication and operation pressures, often reaching hundreds of megapascals.^[11–13] High fabrication pressure is essential to achieve intimate solid–solid ionic contact due to the rigidity of inorganic SSEs, while high operation pressure is applied to counteract the volume expansion of electrode materials, ensuring solid–solid interface contact during charge and discharge processes. Unfortunately, these high pressures are unsuitable for the industrial application of ASSBs. In recent years, many effective strategies have been proposed to tackle the pressure-related challenges of ASSBs.^[14–16] At the material level, Y. Hu et al. developed a viscoelastic SSE with a low elastic modulus of 1.5 GPa, enabling the successful operation of ASSBs at pressures below 0.1 MPa.^[17] At the interface level, innovations such as a self-regulated carbon interlayer with a densification strain of 89% have allowed the operation of anode-free ASSBs at pressures as low as 7.5 MPa.^[18] At the system level, the introduction of a constant pressure spring with a spring rate of 5.5 lb mm^{-1} minimized stress effects, enabling ASSBs to achieve high critical current density at 5 MPa.^[19,20] Additionally, operating ASSBs at elevated temperatures (e.g., 80 °C) has been shown to reduce the necessary operating pressure to 2 MPa.^[14] Therefore, understanding the coupling effect of pressure and electrochemistry is essential when designing high-performance ASSBs.

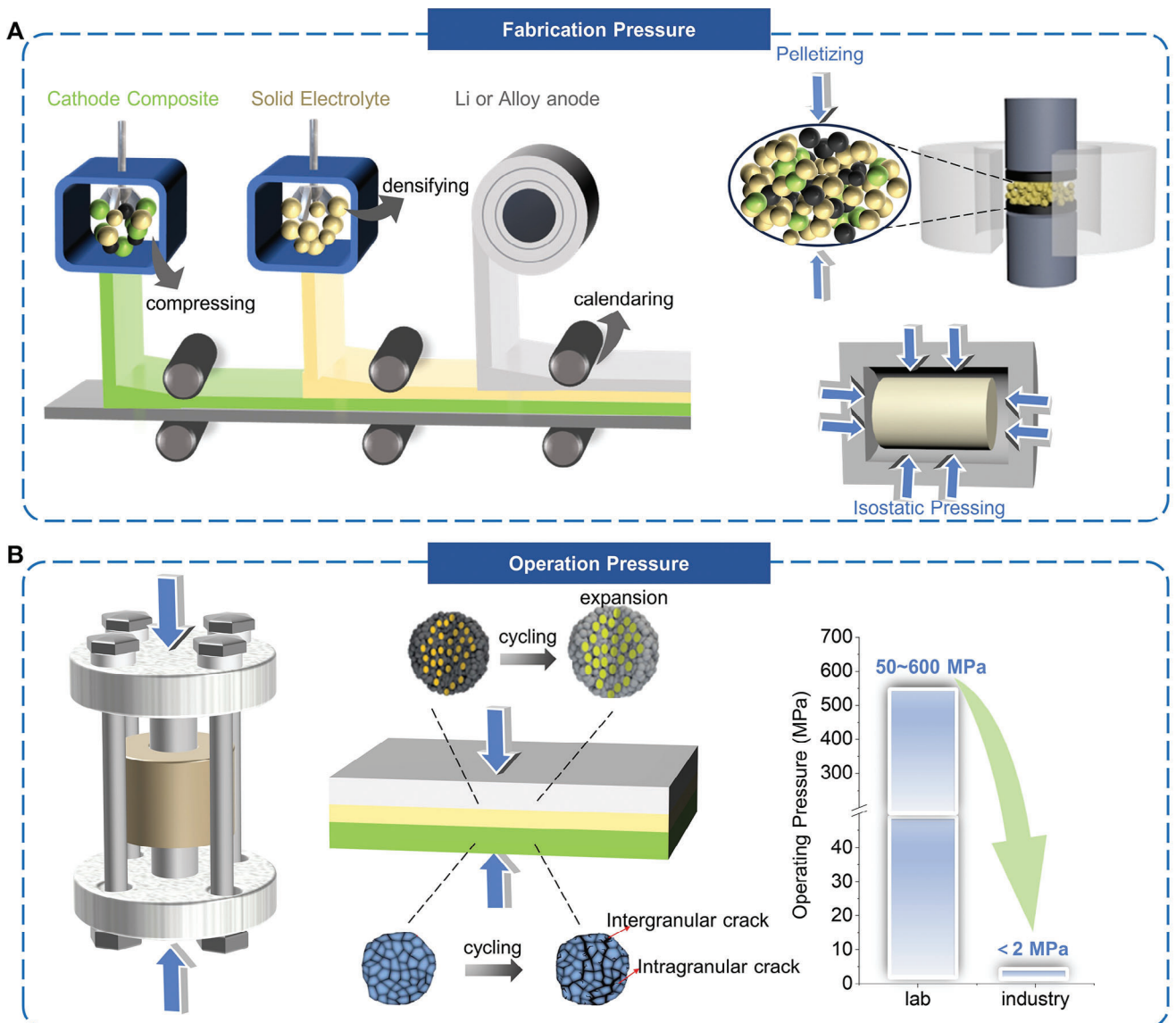


Figure 1. Schematic of the categories and origins of pressure-related challenges of ASSBs. A) Fabrication pressure refers to the externally applied pressure during compressing, densifying, and calendaring. B) Operation pressure signifies externally applied pressure during the battery cycling. Lower middle parts: Adapted with permission.^[21] Copyright 2021, Elsevier. Upper middle part: Adapted with permission.^[22] Copyright 2016, The Royal Society of Chemistry. The operation pressure of ASSBs in most labs is 50–600 MPa, but the target pressure for industry is less than 2 MPa.

This review first clarifies the categories, origins, and challenges of pressures during the fabrication and operation of ASSBs. Then, it summarizes research progress related to pressure issues in ASSBs, focusing on anode and cathode interactions with different SSEs. Various emerging strategies for designing low-operation-pressure ASSBs, crucial for practical engineering, are highlighted. Finally, potential strategies to reduce fabrication and operation pressures based on an understanding of electro-chemo-mechanical failure mechanisms are outlined. This review aims to provide valuable insights into the external pressure effect on ASSBs, guiding academia and industry in designing low-operation-pressure ASSBs.

2. The Category, Origin, and Challenge of Pressure

2.1. Category and Origin of Pressure in ASSBs

The fabrication and operation of ASSBs involve numerous high-pressure processes. For simplicity, these pressures can be categorized into two types: fabrication pressure and operation pressure, as illustrated in Figure 1.

Fabrication pressure refers to the externally applied force during the preparation of electrodes and electrolytes, such as compressing, densifying, calendaring, and pelletizing (Figure 1A). It usually stems from the resistance of different SSEs to

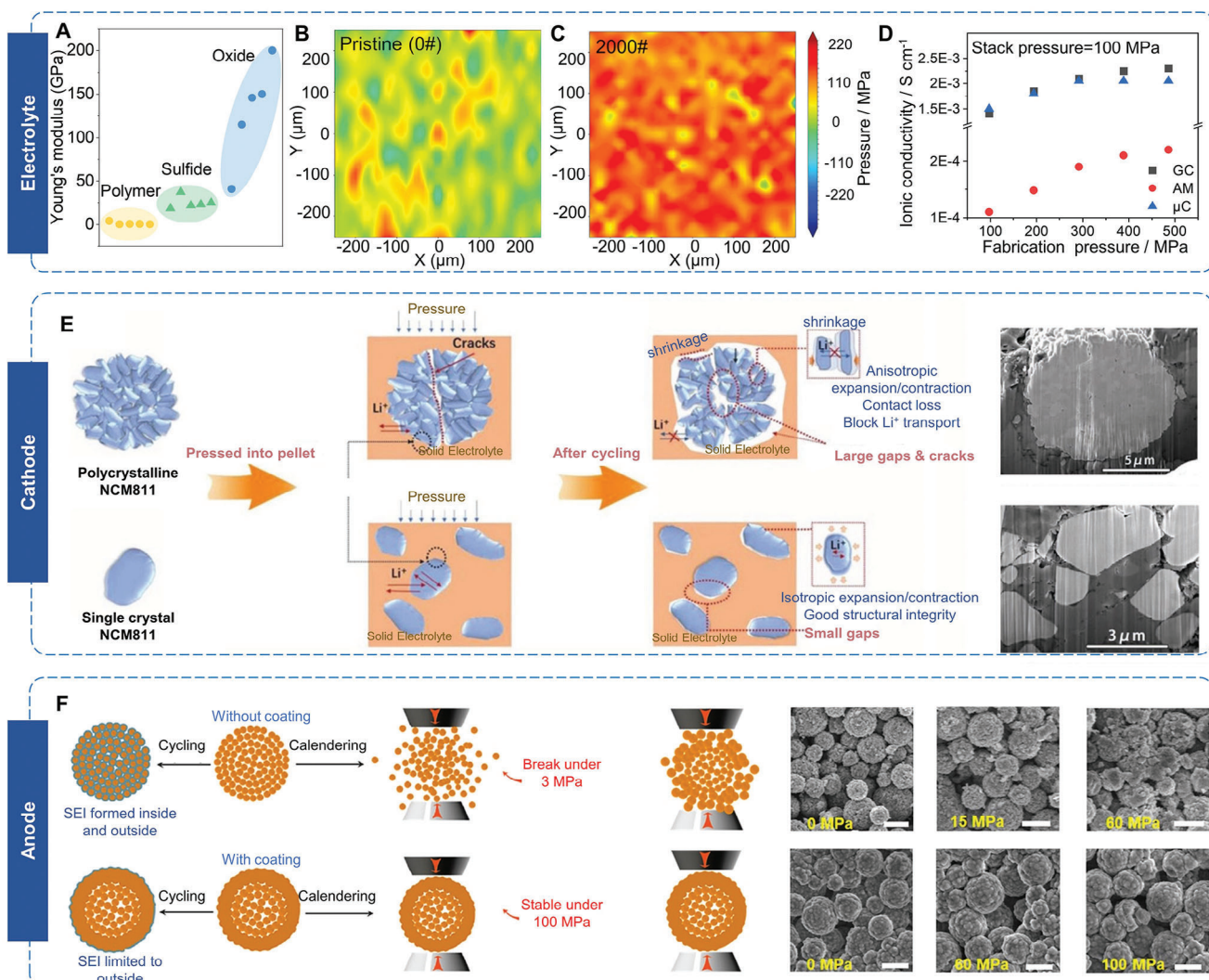


Figure 2. Fabrication pressure for electrolytes, cathodes, and anodes in ASSBs. A) Young's modulus of different electrolytes, data obtained from ref. [22–36] B) Simulating the surface stress distribution of the pristine garnet solid-state electrolyte pellet. C) Simulating the surface stress distribution of the polished garnet solid-state electrolyte pellet. B,C) Adapted with permission.[39] Copyright 2022, The Authors. Published by Elsevier. D) The effects of fabrication pressure on the ionic conductivity of different solid electrolytes, adapted with permission.[50] Copyright 2021, American Chemical Society. E) The response of different crystal types of NCM to fabrication pressure, was reproduced with permission.[51] Copyright 2021, Wiley-VCH GmbH. F) Silicon electrodes with/without a protective coating under high fabrication pressure, reproduced with permission.[52] Copyright 2018, American Chemical Society.

deformation (Young's modules), as shown in **Figure 2A**. Generally, polymer SSEs exhibit lower Young's modulus compared to other types of SSEs. For instance, the pure PMMA has a Young's modulus of ≈ 4 GPa, while the pure PEO has ≈ 82 MPa, depending on its crystallinity.^[23,24] In addition, the addition of salts and plasticizers in polymers also influences their Young's modulus (e.g., 690 MPa for PEO-LiCF₃SO₃,^[25] 519 MPa for PMMA-LiCF₃SO₃,^[26] 160 MPa for PAN-LiClO₄).^[27] In contrast, sulfide SSEs display higher Young's modulus, such as 18.5 GPa for Li₂S-P₂S,^[28] 22 GPa for Li₂S-P₂S₅-P₂O₅,^[29] 23.3 GPa for Li₂O-Li₂S-P₂S₅,^[30] 37.2 GPa for Li₁₀GeP₂S₁₂,^[31] and 22–30 GPa for Li₆PS₅X (X = Cl, Br, I).^[32] Furthermore, oxide SSEs exhibit the highest Young's modulus. For example, Li_{1.2}Zr_{1.9}Sr_{0.1}(PO₄)₃ has a modulus of 41 GPa,^[33] Li_{1.3}Al_{0.3}Ti_{1.7}(PO₄)₃ exhibits 115 GPa.^[34] Al-

substituted Li₇La₃Zr₂O₁₂ has 145.6 GPa,^[35] Li₇La₃Zr₂O₁₂ has a modulus of 150 GPa,^[36] and Li_{0.33}La_{0.57}TiO₃ reaches 200 GPa.^[37] The higher Young's modulus of SSEs, the greater the fabrication pressure required to establish intimate solid-solid interface ionic contact in ASSBs. Moreover, high fabrication pressure introduces stress within ASSB materials or interfaces, such as work hardening induced by surface treatments and compaction.^[38,39] Overall, fabrication pressure significantly impacts the structural integrity, tap density, ionic and electronic conductivity, and even the material phase composition of composite electrodes and SSEs.^[40,41]

Operation pressure is the applied pressure on ASSBs during the charging and discharging process, as illustrated in **Figure 1B**. It serves to counteract the electrochemo-mechanical failure caused by volume changes of electrodes,^[42,43] interface

evolution,^[44] and the forming of lithium dendrites (which can even reach GPa levels in localized areas).^[45,46] Generally, the operation pressure significantly influences the cycling stability, rate performance, and discharge capacity of ASSBs.^[47–49]

2.2. Challenges of Pressure in ASSBs

Currently, the lab-scale high fabrication pressure of hundreds of megapascals is realized via uniaxial pressure or isostatic pressure devices, which is unfavorable to production efficiency improvement and manufacturing cost reduction. For the lab-scale operation pressure of ASSBs, it is generally realized by external mechanical devices, such as hydraulic presses. However, this approach presents several limitations when scaling up to industrial applications, particularly for larger-area cells like pouch cells. For small-area pellet-type cells ($\approx 1 \text{ cm}^2$) in labs, a small and uniform force can be realized by the hydraulic press machine. However, as the cell area increases, the force required to achieve uniform pressure scales linearly. Such a high force exceeds the strength of metallic materials used for peripheral devices. Meanwhile, this creates difficulties in ensuring consistent and uniform pressure across the entire cell stack. In industrial applications, particularly in pouch cells, the huge and uneven pressure distribution can lead to nonuniform lithium-ion flux, poor contact between layers, and localized stress concentrations, which may result in accelerated degradation and dendrite formation. Therefore, reducing the pressure of ASSBs, especially operation pressure, is essential for their commercialization and widespread application in electric vehicles. To our knowledge, the acceptable operation pressure for original equipment manufacturers (OEMs) is no more than 2 MPa (this value varies slightly for different OEMs), with lower pressure being preferred.

3. Current Research Status

3.1. Fabrication Pressure Effect on ASSBs

3.1.1. Pressure-Induced Residual Stress

Fabrication pressure can induce stress changes in electrode and SSE materials, significantly impacting the electrochemical performance of ASSBs. For instance, different surface treatment methods involve varying fabrication pressures, which influence stress distribution within these materials. For example, Bo et al. analyzed stress distribution on the surfaces of untreated LLZTO samples (Figure 2B), revealing obvious compressive stress on the unprocessed electrolyte surface.^[39] The medium stress was calculated to be 26 MPa, with one-fourth of the mapped region under compressive stress state. After polishing the LLZTO pellet surfaces with different grades of sandpaper, significant changes were observed. As shown in Figure 2C, the average stress increased to 143 MPa for the pellet polished with 2000# sandpaper, with most compressive stress regions transitioning into a tensile stress state, thereby reducing the heterogeneity of stress distribution. Theoretical analysis suggests that this uniform stress distribution on the LLZTO surface could lead to more homogeneous lithium deposition.^[39] A similar conclusion was drawn in another

study, where molecular dynamics simulations indicated that SSE surfaces under residual stress could resist lithium dendrite penetration by preventing surface crack formation due to high compressive stress. Consequently, the formation and propagation of lithium dendrites are effectively curbed.^[53] While progress has been made in understanding the coupling between stress and electrochemical behavior in ASSBs, solid experimental evidence is still lacking. The influence of internal stress on lithium-ion diffusion dynamics and the process of lithium dendrite growth remains insufficiently understood.

3.1.2. Fabrication Pressure on SSEs

The fabrication pressure significantly impacts the electrochemical and physiochemical properties of SSEs, particularly their compact density and ionic conductivity at room temperature. Variations in reported ionic conductivities for the same type of SSEs often arise from differing pressures applied during fabrication or cell operation.^[50] For instance, sulfide SSEs, categorized by their crystallization state into amorphous(AM), glass-ceramic(GC), and microcrystalline types(μ C), exhibit varying responses to fabrication pressure (Figure 2D). For amorphous and glass-ceramic solid electrolytes, increasing fabrication pressure enhances ionic conductivity at an operation pressure of 100 MPa. This enhancement is attributed to the closer contact within the electrolyte particles and between the electrolytes and blocking electrodes under high operation pressures. Higher fabrication pressures also boost the compact density of SSE pellets (e.g., 1.45 g cm^{-3} at 100 MPa and 1.8 g cm^{-3} at 500 MPa), thereby improving particle contact and ion transport. In contrast, the ionic conductivity of microcrystalline SSEs is notably independent of fabrication pressure. Beyond 300 MPa, the ionic conductivity of microcrystalline SSEs remains constant. Moreover, voids and gaps may reappear inside the microcrystalline SSEs pellet after unloading the fabrication pressure, likely due to mismatches in crystal lattice orientations among individual grains.^[50] As a result, the ionic conductivity of microcrystalline SSEs is highly dependent on the operational pressure applied to the tested cell, which helps close gaps and pores between grains. Therefore, pellet annealing is essential to achieve high ionic conductivity in microcrystalline SSEs.

The fabrication pressure is also proven to affect the phase components of the SSEs. Schneider et al. discovered that high fabrication pressures bring about plastic deformation, which affects the proportion of the amorphous second phase in glass-ceramics.^[41] Moreover, it was found that a fabrication pressure of 0.5 GPa is suitable to minimize interfacial resistance and maximize ionic conductivity for glass-ceramic thiophosphates. However, the values are likely to be different for other SSEs with significantly different elastic moduli, necessitating substantial exploration. The porosity of SSEs is also related to the fabrication pressure. The focused ion beam (FIB) 3D reconstruction was used to provide direct evidence of the significant influence of fabrication pressure on the porosity of SSEs, which subsequently impacts the overall performance of batteries.^[54] At lower fabrication pressures (50 MPa), a notable porosity led to elevated grain boundary impedance, which was detrimental to battery performance. In contrast, the capacity retention and rate capability of

assembled ASSB prepared under higher fabrication pressure (370 MPa) exhibited remarkable improvement.

3.1.3. Fabrication Pressure on Cathode Composites

Fabrication pressure also plays a crucial role in the integrity of cathode composites. As illustrated in Figure 2E, the effects of different crystal structures of ternary layered cathode materials like $\text{LiNi}_x\text{Co}_y\text{Mn}_{1-x-y}\text{O}_2$ (NCM) under varying fabrication pressures were examined.^[51] During the pressing process at 510 MPa, both large-particle polycrystalline NCM (LP-NCM) and small-particle polycrystalline NCM (SP-NCM) materials produced many cracks. This cracking occurs because these materials are composed of aggregated primary particles with anisotropies in stiffness and crystal orientation. The interfaces among these primary particles are fragile and often exhibit nonconformal contact. Additionally, after charge–discharge cycles, NCM undergoes significant anisotropic volume changes and lattice mismatches due to the random orientation of the polycrystalline internal grains. This leads to uneven internal strains, further exacerbating crack formation. In contrast, single-crystal NCM (S-NCM), composed of primary particles a few microns in size, retains its particle morphology even under a fabrication pressure of 1020 MPa. After electrochemical cycling, the active materials within the composite electrode maintain good integrity and solid–solid contact with the SSEs. This suggests that S-NCM undergoes more uniform primary particle volume changes, making it more suitable for ASSBs.^[51] In terms of LiCoO_2 , Fell et al. revealed that high-pressure treatment resulted in almost no structural changes and had little impact on its electrochemical performance.^[55] These findings indicate that the same type of cathode materials, depending on their crystal structure, or different cathode materials altogether, respond differently to fabrication pressure.

3.1.4. Fabrication Pressure on Anode

The structure and performance of the anode are closely related to the fabrication pressure. For instance, hollow structure designs are often employed to address the large volume changes associated with silicon anodes, as the preserved hollow space can accommodate these changes during lithiation/delithiation, thereby minimizing electrode damage. However, silicon electrodes with hollow structures are prone to fracturing when subjected to high-pressure calendaring.^[52] Reducing the calendaring pressure can alleviate this issue but leads to lower electrode compaction density and poor contact at the electrode/SSE interface, resulting in reduced volumetric energy density and compromised electrochemical performance. This challenge was addressed by depositing a dense silicon layer on clusters of silicon nanoparticles using chemical vapor deposition.^[52] The protective coating enabled the modified silicon electrode to withstand calendaring pressures exceeding 100 MPa without structural collapse (Figure 2F). In contrast, uncoated silicon electrodes experienced cracking even at a fabrication pressure of just 3 MPa. Different fabrication processes can also induce stress changes in materials, affecting the electrochemical performance of ASSBs. For instance, the fabrication of lithium metal, such as through nanostructuring and

nanopatterning, generates initial stress on the Li metal surface. This modified surface, with its nanostructure and internal stress, can promote uniform lithium deposition during the first cycle, leading to improved battery cycle performance.^[38,56] However, the underlying mechanisms and models explaining the increased cycle life are not yet fully understood.

In summary, fabrication pressure impacts the stress distribution within electrode and SSE materials, as well as the ionic conductivity and phase components of SSEs, and the structural integrity of both cathode and anode materials. While high fabrication pressures can ensure initial solid–solid contact, they may also damage electrode materials, thereby degrading electrochemical performance. Further exploration is needed to better understand the relationship between pressure-induced residual stress and the electrochemical behavior of ASSBs.

3.2. Operation Pressure Effect at the Cathode

Appropriate operation pressure can usually prevent chemomechanical failure of cathode composites caused by volume changes of active materials during the charge/discharge processes.^[57] The specific value of operation pressure is often determined by the stress change and intrinsic properties of the electrode and SSEs. Based on crystallographic data, Figure 3A summarizes the volume changes of LCO and NCM cathode materials with varying states of lithiation.^[58] The partial molar volume for homogenous materials and the apparent partial molar volume for two-phase materials are also summarized in Figure 3B. From the results, it is evident that the volume of most cathode materials contracts during lithium removal, with LCO being a rare exception. In addition, the intrinsic properties of SSEs in cathode composite, such as sulfides, oxides, and polymers, also affect a lot in the choice of appropriate operation pressure. The corresponding optimized strategies have been reported recently, which are discussed respectively.

3.2.1. Pressure on Sulfide-Based Cathode Composites

The microstructure of cathode materials plays a crucial role in the electrochemo-mechanical degradation of sulfide-based cathode composites. Nickel-rich cathode materials like NCM-811, paired with $\beta\text{-Li}_2\text{PS}_4$ solid electrolytes, have been studied to investigate interface changes during the charge–discharge cycles of ASSBs.^[57] It was observed that the active material particles lose close contact with the SSEs due to the volume changes of NCM-811 during electrochemical processes. This loss of contact leads to a decrease in electrochemical activity in subsequent cycles. Continuous application of external pressure has been identified as an effective method to maintain contact between the active material and SSEs, thereby ensuring the reactivation of these materials for future electrochemical reactions. Single-crystal NCM has been shown to outperform polycrystalline NCM in maintaining structural integrity under low operational pressures, as it undergoes less anisotropic volume change during charge and discharge cycles.^[51,64–66] This superior microstructural stability in single-crystal NCM helps mitigate electrochemo-mechanical degradation, reducing the need for high operational pressures to maintain close contact between the cathode and SSEs.

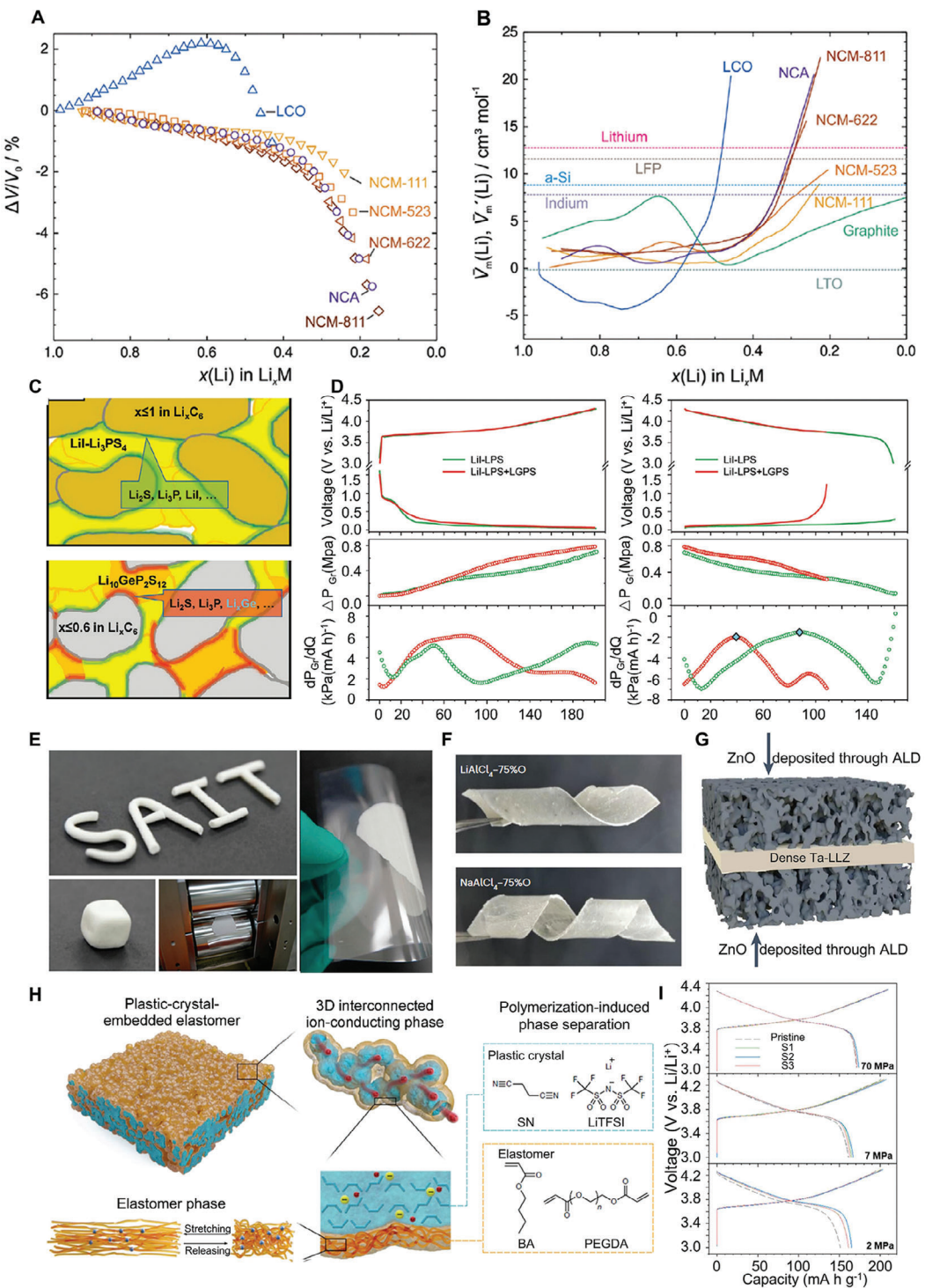


Figure 3. Operation pressure effect at the sulfide-based, oxide-based, and polymer-based cathode. A) The volume changes of LCO and NCM cathode materials with varying nickel content. B) The lithiated molar volume for homogenous materials and the apparent lithiated molar volume for two-phase materials. A,B) reproduced with permission.^[58] Copyright 2018, The Royal Society of Chemistry. C) Schematic illustrated electrodes with/without $\text{Li}_{10}\text{GeP}_2\text{S}_{12}$. D) The electrochemical-mechanical behavior of NCM/Gr full cells with/without reduction-unstable $\text{Li}_{10}\text{GeP}_2\text{S}_{12}$. C,D) reproduced with permission.^[59] Copyright 2020, Wiley-VCH GmbH. E) A material with clay-like characteristics for modifying the oxide-based cathode, reproduced with permission.^[60] Copyright 2021, American Chemical Society. F) Winding membranes of inorganic glass electrolytes with polymer-like viscoelasticity, reproduced with permission.^[17] Copyright 2023, Springer Nature. G) A single-phase mixed ion- and electron-conducting garnet with porous structure, reproduced with permission.^[61] Copyright 2023, Springer Nature. H) The preparation of an elastic polymer solid electrolyte, reproduced with permission.^[62] Copyright 2022, Springer Nature. I) The discharge capacity of solid-state batteries with polymer binders when the operation pressure decreased from 70 to 2 MPa, reproduced with permission.^[63] Copyright 2019, WILEY-VCH GmbH.

Different sulfide SSEs also experience varying degrees of volume change during charge and discharge, influencing the appropriate operation pressure required. As shown in Figure 3C, the lithiation of $\text{Li}_{10}\text{GeP}_2\text{S}_{12}$ led to the formation of Li_xGe alloys, Li_2S , and Li_3P , which have different volumes compared to $\text{Li}_{10}\text{GeP}_2\text{S}_{12}$. This results in the formation of interfacial voids, adversely affecting ionic and electronic contact at the interface. Differential electrochemical pressiometry (DEP) analysis has shown that interfacial side reactions in $\text{Li}_{10}\text{GeP}_2\text{S}_{12}$ significantly impact pressure changes during cycling (Figure 3D).^[59] Thus, high operation pressure is necessary to maintain interfacial contact in the face of substantial volume changes.

Sulfur, as a next-generation cathode material, is highly attractive due to its high theoretical energy density and abundant resources.^[67,68] Moreover, sulfur's chemical compatibility with sulfide-based SSEs makes it particularly advantageous for all-solid-state lithium-sulfur batteries (ASSSBs). Despite these benefits, sulfur's inherent insulating nature and significant volume expansion (up to 80%) during cycling pose challenges that typically necessitate operation under high pressures.^[69] A recent breakthrough involves the design of an $\text{S}_{9.3}\text{I}$ molecular crystal, where iodine (I_2) is inserted into the crystalline sulfur structure, greatly enhancing the material's intrinsic electrical conductivity.^[70] Furthermore, this material exhibits a low bulk modulus of 0.29 GPa (compared to 7.7 GPa for α -sulfur at 25 °C) and a low melting point of ≈65 °C, which is beneficial for repairing interfacial voids by heating. These properties enable ASSSBs to operate stably at a low pressure of 30 MPa. This innovation could inspire further research into other sulfur-based materials with improved mechanical properties. To achieve low-pressure operation of sulfur cathodes, it is crucial to design 3D hosts or elastic binders that can accommodate or manage sulfur's volume changes. These strategies could enable operation at pressures in the tens of MPa range.^[71–73] However, more effective approaches must be developed to reduce the operational pressure to even lower levels, ideally less than 2 MPa, making sulfur cathodes more viable for practical applications in ASSSBs.

3.2.2. Pressure on Oxide-Based Cathode Composites

Forming an intimate solid–solid contact in oxide-based cathode composites poses a significant challenge due to the inherent high hardness and rigidity of oxide SSEs. Typically, a soft functional material is required to enhance interfacial contact in oxide-based SSBs. For instance, a dynamic conformal electrode/SSE interlayer with poly(ϵ -caprolactone) was developed, exhibiting high adhesive strength and distinctive phase-transition characteristics.^[74] The resulting interlayer establishes a dynamic conformal electrode/SSE interface, accommodating the morphological stress-strain of lithium anodes. Even under 0.2 MPa pressure, the symmetric cells remained stable for over 700 h without noticeable voltage polarization. Moreover, under a lower pressure of 0.1 MPa, the capacity of a LiFePO_4 pouch cell with the modified interface retained 85% after 400 cycles. In addition, the porous structure can also effectively release the stress of the stiff oxide SSE. Wachsman et al. developed a single-phase mixed ion and electron conducting (MIEC) garnet with comparable Li-ion

and electronic conductivities (Figure 3G).^[61] The porous structure of the MIEC garnet is crucial in mitigating stress on the solid electrolyte during cycling. By uniformly distributing the voltage potential across the surface, the garnet prevents localized hotspots that can trigger dendrite formation. Consequently, cells constructed with this technology achieve normal cycles without external pressure. Current densities of 100 mA cm⁻² were applied for extended periods without short circuits or degradation, representing the highest achieved for garnet SSEs at room temperature. Therefore, combining soft or porous structures with stiff oxide SSEs is essential for achieving low-pressure operation in solid-state batteries.

3.2.3. Pressure on Other Types of Inorganic-SSEs-Based Cathode Composites

Some newly developed soft inorganic SSEs have displayed promising application potential in low-pressure ASSSBs. Their high deformability facilitates intact contact under low external pressure.^[75] For instance, a clay-like SSE has been employed in constructing ASSSBs (Figure 3E). At room temperature, this clay-like SSE, comprising GaF_3 and 2LiCl, exhibits exceptionally low Young moduli (<1 MPa), a low glass transition temperature of –60 °C, and high lithium-ion conductivity of 3.6 mS cm⁻¹.^[60] When used to build the interface between the cathode layer and stiff oxide SSE layer, this clay-like material ensures full immersion of the cathode within the SSE, guaranteeing intimate ionic contact between them. Consequently, no external operating pressure is required during the operation of ASSSBs. More recently, a class of viscoelastic inorganic glass (VIGLAS) was designed by replacing chlorine of tetrachloroaluminates with oxygen (Figure 3F). Its exceptional mechanical properties, including deformability and low melting temperature, make it suitable for rolling and melt infiltration assembly processes. Additionally, the VIGLAS displays good chemomechanical compatibility with $\text{LiNi}_{0.6}\text{Co}_{0.2}\text{Mn}_{0.2}\text{O}_2$ cathodes, and the low-stacking-pressure (<0.1 MPa) ASSSBs were successfully developed.^[17]

3.2.4. Pressure on Polymer-Based Cathode Composites

Polymer electrolytes, owing to their flexibility and deformability, display significant advantages for achieving low-pressure operation of ASSSBs.^[76] A novel polymer elastic SSE with a 3D interconnected plastic crystal phase was reported.^[62] Through polymerization-induced phase separation, the plastic crystal SN is combined with lithium salt LiTFSI, forming a plastic ion conductor with high ionic conductivity. In-situ crosslinking using azobisisobutyronitrile and polyethylene glycol diacrylate as thermal initiators and crosslinking agents results in the encapsulation of the ionic conductor by the elastic material, leading to the formation of an elastic polymer solid electrolyte (PCEE), as depicted in Figure 3H. The PCEE exhibits exceptional mechanical properties and high ionic conductivity (1.1 mS cm⁻¹ at 20 °C) with a lithium-ion transfer number of 0.75. The in situ formed PCEE within the battery, referred to as “Built-in PCEE,” effectively accommodates volume changes during charge–discharge

cycles. Consequently, the Li|Built-in PCEE|LiFePO₄ full cell maintains a discharge capacity of 93 mAh g⁻¹ at 1C over 1000 cycles at 20 °C, with minimal capacity fading (0.005% per cycle). Subsequently, Han et al. further improved the PCEE by establishing an optimal ratio between the elastic phase and the plastic crystal phase.^[77] They assembled the optimized PCEE with a 35 μm thick lithium anode and a high-loading NMC cathode, demonstrating a remarkably high energy density of 437 Wh kg⁻¹. Polymer binders also offer advantages for enabling ASSBs to operate under low external pressure. A scalable in situ processing approach was developed for polymer binders, where sulfur was employed for in-situ crosslinking sulfuration of polybutadiene rubber, creating a crosslinked structure with elasticity.^[78] Assembled batteries exhibited similar discharge capacity even as the operating pressure decreased from 70 to 2 MPa, as shown in Figure 3I. A mid-polarity solvent (dibromomethane) was applied to co-polymerize Li₆PS₅Cl with an ionic liquid and nitrile butadiene rubber, resulting in an electrolyte with excellent mechanical properties suitable for large-scale production.^[63] Additionally, a gel-like lithium-ion conductor binder, prepared by blending Pyr₁₄TFSI, LiTFSI, and PEO, fills the sulfide electrode during the coating process, enhancing both the interface contact area and bonding strength. Importantly, the binder accommodates the volume expansion of the active material during cycling.^[79]

In brief, an appropriate operation pressure is generally required to prevent the electrochemo-mechanical failure of cathode composites in ASSBs. The sulfide solid electrolytes generally need high operation pressure to achieve high lithium-ion conductivity. In addition, the volume change caused by the interfacial reactions between the cathode and SSEs should also be considered. As for the fragile oxide SSEs, the operation pressure is much lower than that of sulfide. However, designing soft materials or porous structures is essential for achieving low-pressure operation of oxide SSE-based ASSBs. Polymer electrolytes display significant advantages for achieving low-pressure operation of ASSBs due to their flexibility and deformability. However, the lithium-ion conductivity and electrochemical stability need further improvements. Overall, mechanical failure primarily arises from the volume changes in electrode materials and interface evolution. Designing low-operation-pressure ASSBs requires full consideration of factors such as the mechanical properties of electrode materials, the chemical and electrochemical stability of SSEs, and the chemical compatibility between inorganic and organic materials.

3.3. Operation Pressure Effect at the Anode

Compared to cathode materials, which generally undergo intercalation reactions with small volume change (<10%) during cycling,^[80,81] anode materials such as lithium metal, Li-Mg alloys, and Si undergo conversion or alloying reactions, resulting in significant volume changes (>100%).^[82] The volume of the anode expands considerably during lithium deposition or lithiation, potentially generating high compressive stress on the order of 10⁻¹ GPa on the anode side.^[83] This rapid build-up of local stress can even cause cracks in single-crystal electrolyte particles.^[84] These stress and volume changes pose critical challenges for the low-pressure operation of ASSBs.

3.3.1. Pressure on Lithium Metal Anode

Lithium metal exhibits good ductility at room temperature, making it prone to deformation under external pressure. Therefore, its electrochemical performance is significantly influenced by the stacking pressure.^[91] The electroplating/stripping process of lithium metal symmetric cells under different operating pressures has been investigated.^[85] In Figure 4A, at an operating pressure of 5 MPa, lithium metal maintains good contact with SSEs during cycling without creeping and dendrite formation. Symmetric cells cycled for over 1000 h without any short circuits. When the operating pressure is increased to 25 MPa, lithium metal slowly creeps into the interior of the electrolyte from surface pores but without penetrating it. The protrusion of lithium metal into SSEs reduces the distance between the two electrodes, lowering the initial overpotential and becoming a preferential site for lithium plating once the plating-stripping process begins. After 48 h of plating-stripping, continuous extension of lithium dendrites leads to battery failure. Upon further increasing the operating pressure to 75 MPa, lithium metal mechanically creeps through the entire SSEs without undergoing any plating-stripping process. This results in severe cracking of SSEs. The explanation lies in the fact that 75 MPa exceeds the yield strength of lithium metal by a hundredfold, and the electrolyte, with 18% porosity, is not dense enough, providing space for lithium metal creep.

In a recent study, Bruce et al. investigated the influence of applied pressure on the generation and propagation of lithium dendrites.^[86] The simulation of lithium dendrite growth during a plating/stripping cycle at a given capacity revealed that the length of dendrite growth varies with the applied operating pressure, as depicted in Figure 4B. At operating pressures approaching zero, the growth of lithium dendrites is nearly negligible. Conversely, at higher pressures, such as 7 MPa, the pressure encourages lithium metal to extrude against the electrolyte, resulting in increased lithium dendrites and rapid crack propagation. To experimentally validate their findings, the researchers assembled a three-electrode Li/Li₆PS₅Cl battery. During electroplating at a current density of 4.0 mA cm⁻² under an operating pressure of 0.1 MPa, the voltage gradually decreased in the initial cycles, indicating lithium penetration into the electrolyte and reduced battery impedance. However, the battery experienced a short circuit after cycling 170 times. In contrast, under an applied pressure of 7 MPa, the battery short-circuited after only 35 cycles, underscoring that higher pressure leads to faster short-circuiting. The high ductility of lithium metal highlights the importance of stress relief to achieve dendrite-free ASSBs. The evolution of the Li|Li₂La₃Zr₂O₁₂ (LLZO) interface was observed using in-situ transmission electron microscopy (TEM).^[45] Under strong mechanical constraints and low charging rates, the stress induced by lithium-ion deposition leads to lateral expansion of lithium metal on LLZO. However, during rapid lithium plating, the rapidly accumulating local stress reaches at least GPa levels, swiftly causing nearly defect-free LLZO particles to fracture.

Integrating a soft substrate or inducing a porous layer proves to be an effective strategy for relieving stress changes and providing space for lithium deposition. For instance, a soft polydimethylsiloxane (PDMS) substrate was combined with Li foil to create a stress-adaptive interface between Li and a garnet

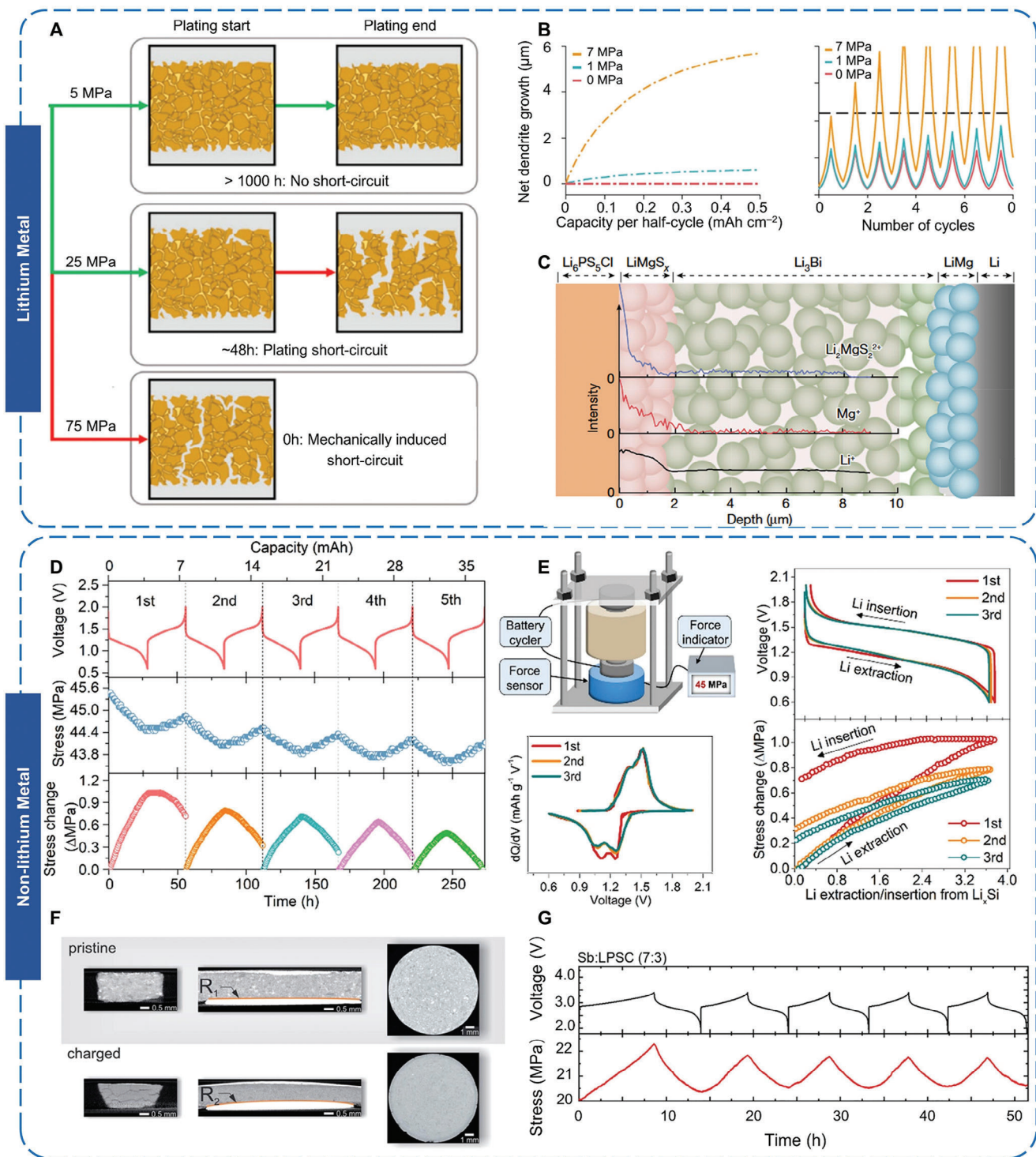


Figure 4. Operating pressure effect at lithium metal anode and non-lithium metal anode. A) The electroplating/stripping process of lithium metal symmetric cells under different operating pressures, reproduced with permission.^[85] Copyright 2019, WILEY-VCH GmbH. B) The influence of applied pressure on the generation and propagation of lithium dendrites, is reproduced with permission.^[86] Copyright 2023, Springer Nature. C) Distributions of elements along the depth of the $\text{Mg}_{16}\text{Bi}_{84}$ to the Li anode, reproduced with permission.^[87] Copyright 2023, Springer Nature. D) The pressure variation during the full cell cycling process. E) The dQ/dV curve during the cycle and the stress changes corresponding to lithium extraction and insertion. D,E) reproduced with permission.^[88] Copyright 2022, Elsevier. F) X-ray computed tomography (CT) scans on LCO/SSE/LiIn batteries before and after charge, reproduced with permission.^[89] Copyright 2017, The Royal Society of Chemistry. G) The stress changes in the Sb anode during electrochemical cycling, were reproduced with permission.^[90] Copyright 2021, Elsevier.

electrolyte.^[92] This highly elastic PDMS allows for continuous compressive stress release. During the plating/stripping process, the contact between the lithium metal anode and the garnet-type electrolyte is mechanically improved, resulting in a stabilized interface. This, in turn, helps alleviate local stress and uneven ion flux distribution during cycling, suppressing the formation of lithium dendrites. The PDMS/Li symmetric cell demonstrated stable cycling for over 5000 cycles with an ultra-low overpotential of 55 mV at 0.2 mA cm⁻². In another development, Wang et al. created the Mg₁₆Bi₈₄ interlayer at the Li/Li₆PS₅Cl interface, as depicted in Figure 4C. During cycles, the interlayer transforms into a LiMgS_x–Li₃Bi–LiMg multifunctional structure.^[87] The porous Li₃Bi layer allows lithium to grow into it, relieving stress changes. Hence, at a low operating pressure of 2.5 MPa, the assembled full cell achieves a capacity of 11.1 mAh⁻² with a cell-level energy density of 310 Wh kg⁻¹.

3.3.2. Pressure on Nonlithium Metal Anode

Alloy anodes that form lithium intermetallic compounds often undergo significant volume changes, resulting in poor structural stability.^[93] Maintaining the interface between the anode and SSEs typically requires high stacking pressure. Silicon anodes exhibit a high specific capacity of 3579 mAh g⁻¹ and can accommodate 3.75 mol of lithium per mole of silicon. However, they undergo a significant volume expansion of 300% during the lithiation process.^[94–98] The substantial volume expansion results in severe cracking and pulverization during cycles, contributing to poor electrochemical performance. The volume change of micro-sized μ -Li_xSi electrodes has been investigated during cycling.^[88] A μ -Li_xSi|SSE|Li₄Ti₅O₁₂ full cell was assembled, with the Li₄Ti₅O₁₂ (LTO) cathode serving as a typical “zero-strain” electrode. Figure 4D depicts the pressure variation during the full cell cycling process, primarily attributed to pressure changes induced by μ -Li_xSi. The corresponding dQ/dV curve is presented in Figure 4E. Across the cycling process at an area capacity of 3 mAh cm⁻², the full cell showed stress fluctuations of \approx 0.7 MPa. Stress decreases during discharge and increases during charge, aligning with lithium extraction and insertion in the electrode. Theoretically, stress changes depend solely on the variation of lithium content within the μ -Li_xSi electrode. However, the presence of some electrode-electrolyte gap and possible elastic deformation may mitigate stress changes. Thicker electrolytes result in smaller strain. Additionally, as LTO may irreversibly capture some active Li during the first cycle, stress hysteresis might occur but is expected to disappear in subsequent cycles.

For the In anode, the formation of the In-Li alloy phase leads to volume expansion of the electrode, causing stress changes. Janek and his colleagues conducted X-ray computed tomography (X-CT) scans on LCO/SSE/In-Li batteries before and after charging (Figure 4F). They observed significant bending of the ASSB after charging, especially at the electrode/electrolyte interface, where the strain was pronounced.^[89] Additionally, the increasing pressure during charging resulted in a more uniform pore distribution for the solid electrolyte, making it denser. However, the pressure also induced noticeable cracks at the edges of the electrolyte, causing contact loss. Therefore, if the battery is not subjected to external pressure during cycling, electrode expansion could

prevent tight contact between the electrode and electrolyte, ultimately leading to battery failure. Stress changes in the Sb anode during electrochemical cycling were monitored (Figure 4G).^[90] The pressure increased with charging and decreased with discharging. After completing charge–discharge cycles, a substantial pressure of 2.25 MPa was generated. This phenomenon was also observed in Sn and Si electrodes.^[54] Additionally, the rate of stress increase was found to be nonlinear, attributed to the initial structure adjusting at the beginning of cycling for the electrode. Irreversible changes in electrode thickness occurred after five full cycles, and internal damage was observed within the electrode.

In contrast, metals that form solid solutions with lithium demonstrate higher structural stability, which is advantageous for the low-pressure operation of ASSBs. Asakura et al. investigated sulfide glass electrolytes paired with lithium metal or Li-Mg alloy electrodes, examining the impact of operating pressure on the lithium stripping/plating process.^[99] Their findings revealed that the use of Li-Mg alloy allowed the battery to cycle at higher current densities with lower operating pressure. This improvement is due to the formation of a lithium-removed porous structure that remains at the electrode/electrolyte interface after significant Li stripping, preserving the conduction pathways for Li⁺ ions and electrons while suppressing void formation at the interface. Similarly, Li-Ag solid solution alloys also exhibit robust structural stability, making low-pressure operation more feasible.^[100,101] Building on this concept, reduced graphene oxide (rGO) was utilized to develop an rGO/Li-Ag anode composite. The nanoscale rGO host ensures uniform SSE/anode interfacial contact and the solid-solution nature of the Li-Ag alloy facilitates the cyclic refilling of the rGO host during cycling. These combined effects effectively maintain the interfacial connection even at low pressure, enabling stable cycling at an operating pressure of just 4.9 MPa.^[102]

3.3.3. Pressure on Anode-Free ASSBs

Anode-free ASSBs have garnered significant attention due to their enhanced energy density and inherent safety.^[105] However, operating these cells at low pressure is challenging due to slow reaction kinetics and interfacial contact loss during lithium stripping and plating. A critical factor in enabling anode-free ASSBs is the interlayer between the SSE and the current collector, which mitigates volume changes. As depicted in Figure 5A, compared to the bare Cu electrode, Ag- and Au-modified electrodes exhibit lower total resistance at the end of Li stripping, owing to reduced contact loss. The alloy interlayer helps to homogenize the current around Li islands during the final stages of stripping by counteracting localized delithiation driven by increased overpotential.^[106] This enhances the resilience and stability of the anode/SSE interfaces. The use of a Mg layer, which facilitates reversible Li plating and stripping via a (de)alloying reaction with minimal volume change, has been validated.^[99] Jang Wook Choi et al. developed MXene as a pressure buffer layer to prevent void formation at the interface.^[103] As shown in Figure 5B, a composite thin film comprising a Mg upper layer and a Ti₃C₂T_x MXene buffer layer was introduced to anode-free ASSBs, successfully maintaining the SSE/electrode interface even at a low operating pressure of 2 MPa. Additionally, an elastic binder, composed of

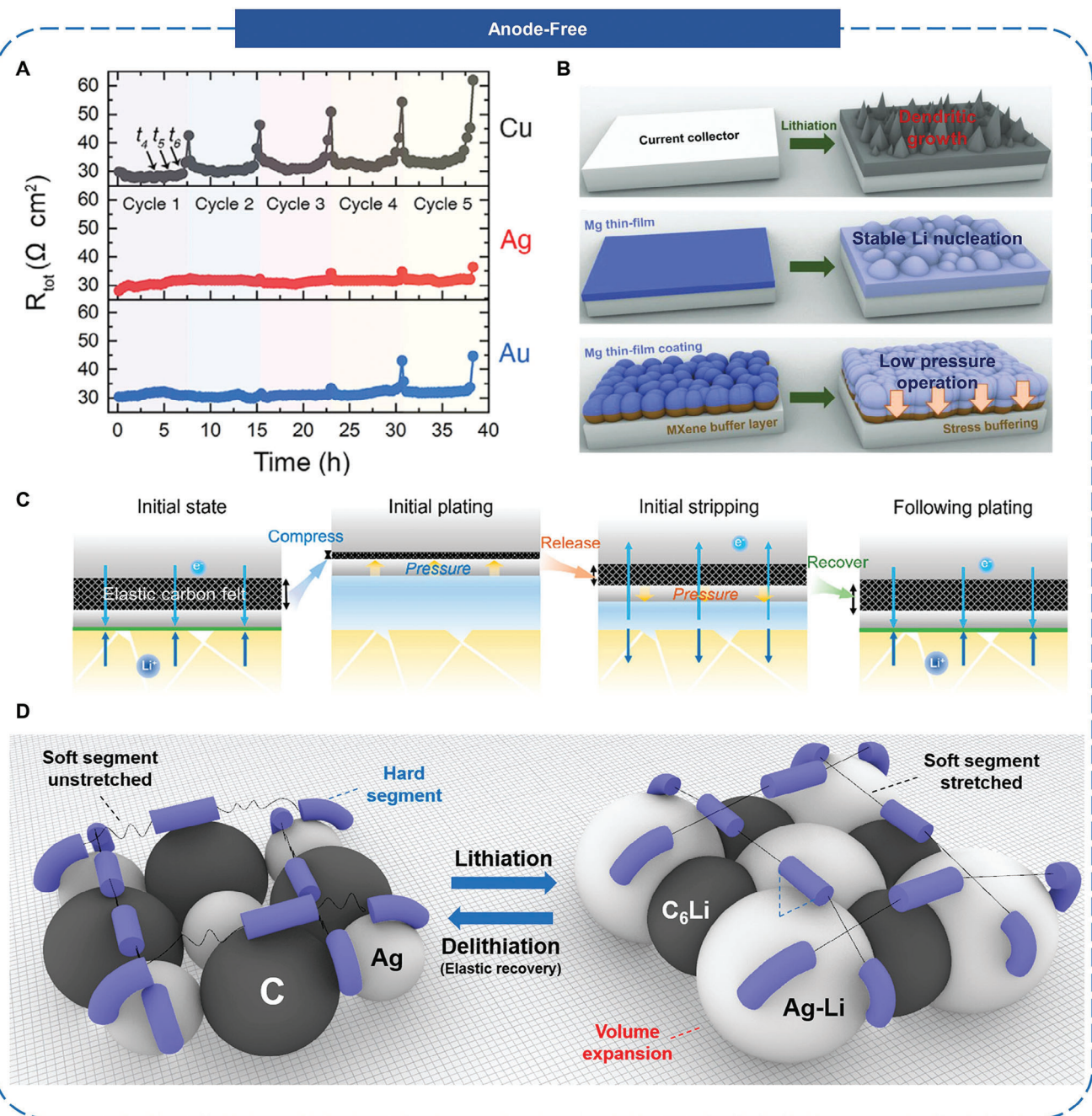


Figure 5. Operating pressure of anode-free ASSBs. A) Li plating on the bare current collector, Mg film, and Mg/ MXene double-layer, reproduced with permission.^[98] Copyright 2024, Springer Nature. B) Total resistance measured over five cycles for Cu, Ag, and Au electrodes, reproduced with permission.^[103] Copyright 2023, WILEY-VCH GmbH. C) Schematic illustration of anode-free ASSBs with self-regulated pressure during cycling, reproduced with permission.^[18] Copyright 2023, American Chemical Society. D) A graphic illustration of the elastic recovery of Ag particles during lithiation/delithiation, reproduced with permission.^[104] Copyright 2022, American Chemical Society.

soft and hard segments, was developed based on a silver-carbon composite.^[104] The soft segments engage in strong hydrogen bonding with the active material, while the hard segments promote the elastic adjustment of the binder network (Figure 5D). These innovations have significantly improved the mechanical stability and long-term cyclability of ASSBs, making low-pressure operation more feasible. Moreover, an elastic interlayer can be ef-

fective in ensuring consistent SSE/electrode contact. Zhu et al. designed a conductive carbon-felt elastic layer on the anode side that self-adjusts the pressure.^[18] This conductive elastic layer not only supports uniform Li deposition but also alleviates stripping/plating stress (Figure 5C). As a result, the initial Coulombic efficiency increased significantly from 58.4% to 83.7%, along with improved cycling stability for anode-free ASSBs.

In brief, lithium metal facilitates low operation pressure due to its high deformability. Non-lithium metal anodes, particularly those forming lithium intermetallic compounds, generally require higher operating pressures to handle significant volume expansion and maintain good contact with the SSE. Conversely, metals that form solid solutions with lithium offer better performance at low pressures, thanks to their structural stability. For anode-free ASSBs, the common issue is the lack of tight contact between the current collector and the rigid SSEs. Therefore, designing an elastic interlayer at the anode/SSE interface is essential for achieving stable and low-pressure operation in anode-free ASSBs.

4. Characterization and Simulation

To better understand the pressure-associated effects in ASSBs, advanced characterization, and simulation are of great importance. Various in-situ imaging and spectroscopy methods, along with simulation methodologies, have been employed to study these effects, enhancing the fundamental understanding and guiding the rational design of low-pressure ASSBs. A millimeter-sized battery designed for in situ characterization is illustrated in Figure 6A. The laboratory X-ray computed tomography (XCT) results reveal the presence of longitudinal cracks within the original electrolyte bulk,^[107] and after cycling, numerous transverse cracks were observed within the solid electrolyte. Further investigations on a Li₆PS₅Cl/Li₁₀GeP₂S₁₂/Li₆PS₅Cl sandwich electrolyte using XCT demonstrated an increased transverse interfacial crack in multi-layer solid electrolytes after cold pressing and cycling. The different mechanical properties of SSE layers, such as varying Poisson's ratios, induced distinct lateral displacements, resulting in transverse crack patterns at interfaces and potentially suppressing dendrite formation under vertical external pressure. Raman spectroscopy was employed on LLZTO subjected to varying pressures, enabling the acquisition of characteristic Raman peaks.^[39] A Python program transformed the measured Raman spectral peaks into stress values, generating a 2D stress map (Figure 6B). This approach allowed for visualizing and characterizing stress distribution across LLZTO, providing valuable insights into its mechanical behavior under different pressures. The tested plane could be adjusted along the z-axis for a 3D stress mapping. Other than imaging and spectroscopy methods, the theoretical model is also very important for understanding the interfacial stress of ASSBs. Recently, the stress-related formula was established based on the previously reported model,

$$P_i = \frac{\epsilon_{Cu} E_{Cu}}{1 - \nu_{Cu}} \times \left\{ \frac{3(r_i + t)^3}{2[(r_i + t)^3 - r_i^3]} - \frac{\nu_{Cu}}{1 - \nu_{Cu}} \right\} \quad (1)$$

where P_i represents the stress in Li/Cu interface, ν_{Cu} and E_{Cu} are Poisson's ratio and Young's modulus of Cu, respectively. And ϵ_{Cu} is the circumferential strain, t and κ represent the thickness and curvature of Cu, r_i is the radius of the hypothetical lithium sphere.^[108] It was observed that as the strain of the copper current collector increased from 0.024 to 0.052, the stress in copper rose from 0.151 to 0.503 GPa. Notably, this stress is two orders of magnitude higher than the externally applied pressure on the battery, as illustrated in Figure 6C. The high interfacial

stress effectively restricts the morphology of lithium metal, enabling compact deposition of lithium metal even under zero external pressure. Furthermore, it is evident that interfacial stress is directly proportional to the strain of the copper current collector and inversely proportional to the diameter of the hump during lithium plating. This implies that stress is applied to lithium metal during vertical growth, guiding it to grow horizontally and release stress. A comprehensive model, involving various polymer coatings, was established to emphasize the correlation between interfacial impedance and operating pressure, and coating thickness.^[76] Machine learning, coupled with high-throughput computations, was employed to derive the optimal combination of pressure and polymer coating thickness. This approach provides insights into optimizing the performance of the interface between lithium metal and polymer electrolyte layers under different pressures. Density Functional Theory (DFT) was applied to predict the decomposition reactions of SSEs and the associated volume changes.^[44] It was found that stress changes associated with the decomposition of SSEs may be more significant than those of the electrode during lithium insertion/extraction. This underscores the importance of considering the mechanical effects of SSEs decomposition in the overall performance of ASSBs.

In summary, advanced in situ characterization and theoretical calculations play a crucial role in understanding pressure-associated effects in ASSBs. There are still ample opportunities to develop new methods for characterization and calculation to further advance the fundamental understanding of these pressure-related effects.

5. Strategies to Reduce the Pressure of ASSBs

In recent research, considerable efforts have been dedicated to understanding the impact of pressure on ASSBs.^[109–114] As a result, effective strategies have been proposed to reduce operating pressure while maintaining high electrochemical performance (relieving the influence of stress and maintaining interfacial contact). Some typical strategies are summarized in Table 1. They can fall into two categories: material design and cell design, which are discussed in the following content.

Material design strategies for ASSBs require a multi-faceted approach. 1) **Surface coating and bulk doping:** Using element diffusion chemistry, a stratified Al/Zr modified Ni-rich cathode was designed with low strain ($\Delta_{volume} \approx 4.15\%$).^[43] This modification, achieved through a layered structure and stabilized lattice elements, effectively alleviated internal stress. While this cathode can operate at 2 MPa, maintaining long-cycle performance at low pressure remains challenging due to residual volume strain. 2) **Integrated electrode design:** Recently, a Li_xTiS₂ cathode free of SSEs was reported.^[115] This design promotes uniform volume expansion and contraction across the entire electrode, unlike composite cathodes where only the active material undergoes these changes. By minimizing contact losses between the electrode and the solid electrolyte, this approach improves overall performance. However, the cathode currently shows poor rate capacities, indicating a need for further improvements in its dynamic properties. 3) **Mechanical equilibrium in cathode composites:** Achieving mechanical equilibrium in materials design can be accomplished by creating a nearly zero-strain composite

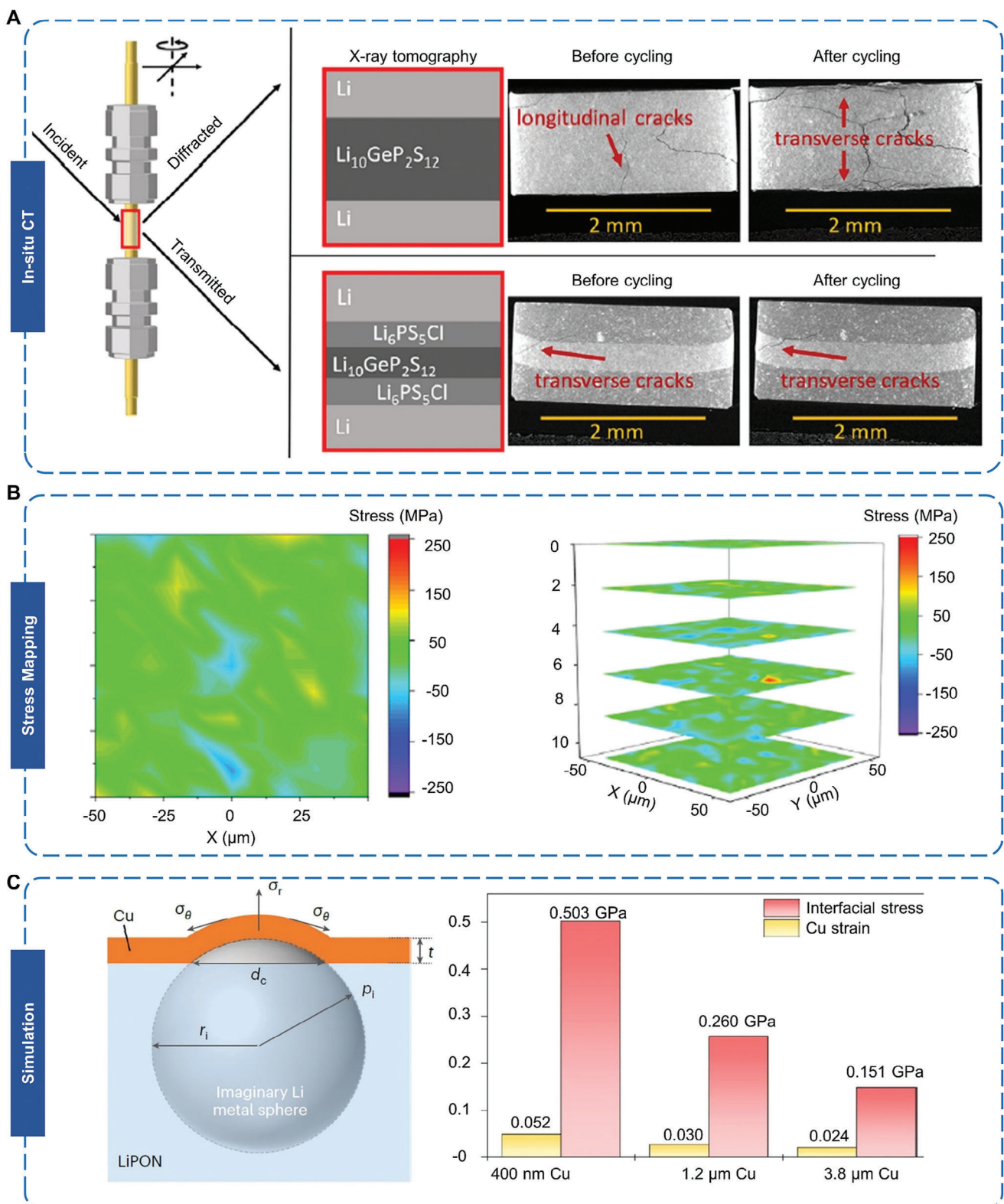


Figure 6. Advanced Characterization and Simulation about Pressure-Induced Behavior in ASSBs. A) A millimeter-sized battery designed for in situ XCT characterization, reproduced with permission.^[107] Copyright 2022, American Chemical Society. B) The 2D/3D stress map from the Raman spectrum. Adapted with permission.^[39] Copyright 2022, The Authors. Published by Elsevier. C) The model of predicting the stress in copper as the strain changes, is reproduced with permission.^[108] Copyright 2023, Springer Nature.

Table 1. State-of-the-art strategies to reduce operating pressure in ASSBs.

Fabrication pressure [MPa]	Operation pressure [MPa]	Strategies	Cell performance	Refs.
360	2	Hierarchical Al/Zr decorated Ni-rich cathode	166.7 mAh g ⁻¹ at 0.2C	[43]
390	0.1	O ₃ -Li _x TiS ₂ , SE-free cathode	165 mAh g ⁻¹ at 0.2C	[115]
445	70	Blending cathode with opposite expansion coefficients	Not Given	[58]
Not Given	0.32	3D lithium-host design	40 mAh at 0.2C charge and 0.4C discharge (pouch cell)	[116]
380	1	Composite anodes	25 mAh cm ⁻² at 0.1 mA cm ⁻²	[117]
500	2	Reduce the cut-off voltage	118 mAh g ⁻¹ at 1 mA cm ⁻²	[20]
500	2	Isostatic pouch cell holders utilizing air	173.6 mAh g ⁻¹ at 0.1C (pouch cell)	[118]
375	5	Incorporating compression springs	0.87 mAh cm ⁻² at 1 mA cm ⁻²	[119]
5	<0.1	Viscoelastic inorganic SSEs	173 mAh g ⁻¹ at 1 C	[17]
Not Given	2.5	Mg ₁₆ Bi ₈₄ interlayer at anode F-rich interlayer at the cathode	11.1 mAh cm ⁻² at 0.25 mA cm ⁻²	[87]

cathode through the combination of materials with opposing expansion coefficients. For instance, blending LCO with NCM in suitable ratios enables these materials to expand and contract independently during cycling, resulting in an overall stress balance (Figure 7A).^[58] This composite cathode demonstrates reduced stress variation throughout the cycling process compared to cathodes made solely from LCO or NCM. Despite alleviating overall stress, maintaining reliable internal contacts among LCO, NCM, and SSEs remains a challenge. 4) **Designing a composite structure for lithium metal anodes:** Addressing the severe volume expansion of lithium metal anodes involves designing structures that constrain the expansion or reduce void formation. For instance, a lithium metal composite anode has been developed by integrating a hollow silver/carbon fiber scaffold with an inorganic/organic composite electrolyte.^[116] This configuration creates a dynamically stable interface with the lithium metal, leveraging the high surface area for improved interfacial contact and using the hollow structure to alleviate stress from lithium plating. Similarly, a composite anode combining carbon nanotubes (CNTs) with lithium metal was created, enhancing lithium atom diffusion and minimizing void formation even under low external pressure.^[117] However, the inclusion of nonactive materials may decrease the anode's energy density, requiring further optimization. 5) **Developing novel electrode binders:** Recent advancements in electrode binders have improved the maintenance of inter-particle interface contacts under low pressures. For instance, vulcanized butadiene rubber was introduced during the wet-slurry fabrication process, forming a mechanically resilient crosslinked structure and achieving a high specific capacity of 150 mAh g⁻¹ even without external pressure.^[78] Additionally, block polymer binders combining ionic conductivity with suitable mechanical properties have been designed.^[24] These binders have been optimized to enhance both electrochemical and mechanical performance, allowing stable cycling at 1 MPa. However, polymer binders often suffer from poor chemical compatibility with inorganic SSEs and limited stability at high voltages, which necessitates further development.

In the aspect of cell design, several effective strategies have been employed to achieve low-pressure operation. 1) **Cut-off voltage and temperature control:** An all-solid-state battery was assembled using LiNi_{0.83}Mn_{0.06}Co_{0.11}O₂ cathode, Li₆PS₅Cl solid electrolyte, and lithium indium (In-Li) anode. To achieve low-pressure operation, the charge cut-off voltage of the battery was controlled, reducing it from the conventional 4.4–4.2 V. This adjustment significantly decreased the volume expansion rate of the cathode from an initial 6–2.5%. The battery exhibited improved capacity retention (from 65% to 94% after 50 cycles) with only a 14% reduction in overall capacity (Figure 7B).^[20] Additionally, increasing the testing temperature was identified as another strategy to achieve high-performance all-solid-state batteries under low operating pressures. Batteries tested under 2 MPa at an ambient temperature of 80 °C displayed higher discharge specific capacity compared to those tested at 30 °C. 2) **Effect of applied pressure direction:** The direction of applied pressure has been found to significantly impact the performance of ASSBs. Adjusting the testing environment to achieve 3D contact between the active material and solid electrolyte has been suggested as a strategy to improve battery performance, particularly under low operating pressures.^[120,118] Recently, a pouch cell holder using air as the pressurizing medium was designed to achieve isostatic operation pressure, confirming that isostatic pressure during cycling is beneficial.^[118] However, the holders may only be suitable for lab-scale testing, and further efforts are needed to realize isostatic pressure operation in commercial batteries. 3) **Utilization of springs in battery molds:** The incorporation of springs in battery molds proved to be an effective strategy. As shown in Figure 7C, critical current density tests were conducted using conventional testing molds equipped with installed springs.^[19] Pressure changes during the battery cycling process were monitored with pressure sensors. Batteries equipped with springs experienced only a 4% increase in pressure (from the initial 5–5.21 MPa after charging), allowing the battery to cycle at higher current densities up to 1.0 mA cm⁻². The strategic cell structure design successfully displays controlled pressure fluctuations during the cycle, mitigating the failure of ASSBs.^[119]

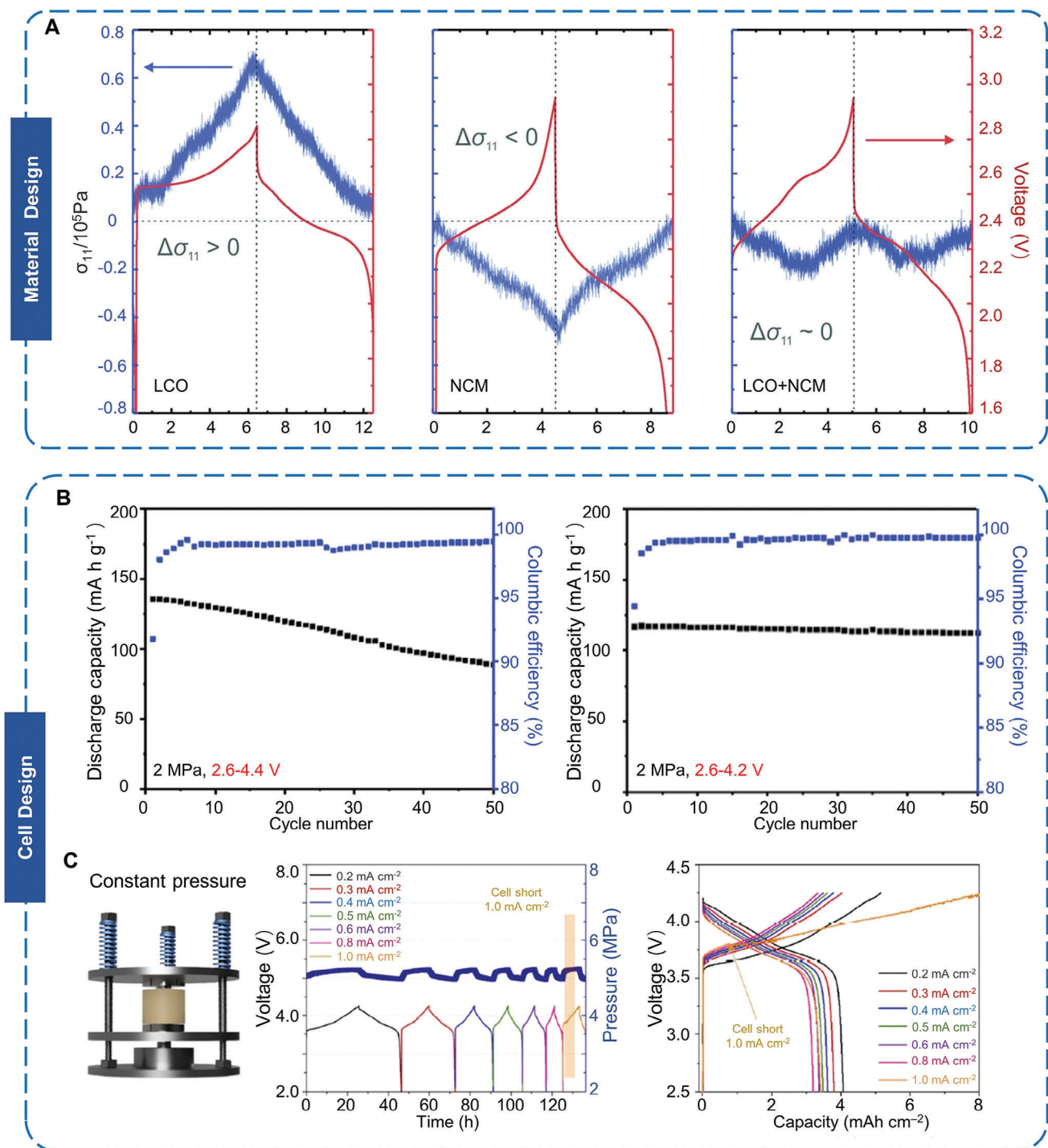


Figure 7. Effective strategies to reduce the operating pressure of ASSBs. A) The pressure changes of LCO, NCM, and LCO/NCM composite cathode during cycling, reproduced with permission.^[58] Copyright 2018, The Royal Society of Chemistry. B) The capacity retention of the battery after reducing the charge cut-off voltage from 4.4 to 4.2 V, reproduced under the terms of the CC-BY Creative Commons Attribution 4.0 International license (<https://creativecommons.org/licenses/by/4.0/>).^[20] Copyright 2022, The Authors. Published by Elsevier. C) Critical current density tests from the conventional testing molds with installed springs, adapted with permission.^[119] Copyright 2024, The Authors. Published by Elsevier.

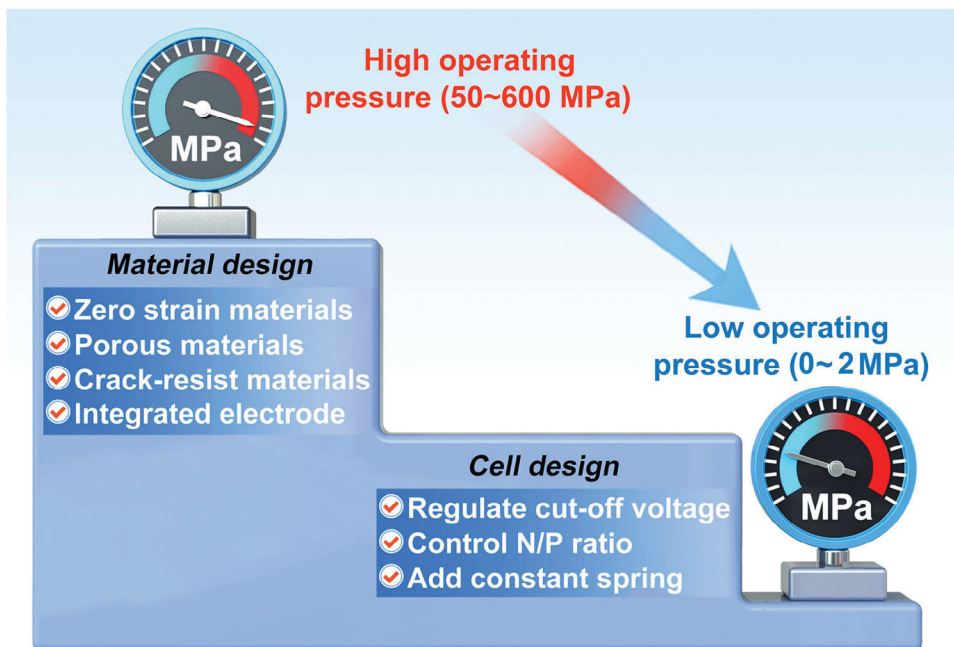


Figure 8. Summary of strategies to reduce the operating pressure of ASSBs.

In summary, achieving lower stacking pressure in all-solid-state batteries (ASSBs) requires a holistic approach that includes careful consideration of materials and electrode structure design, as well as thoughtful battery pack design.

6. Summary and Outlook

In summary, pressure-induced effects in ASSBs have garnered increasing attention recently. This review categorizes pressure in ASSBs into two types: fabrication pressure and operation pressure. Fabrication pressure refers to externally applied pressure during electrode and SSE fabrication, while operation pressure involves continuously applied external pressure during battery operation. Additionally, a summary of the current research status regarding pressure-related issues in ASSBs is provided. The impact of fabrication pressure on SSEs, cathode materials, and anode materials is discussed, alongside the effects of operation pressure on both cathode and anode composites with typical SSEs, including sulfides, oxides, and polymers. Advanced characterizations such as *in situ* CT, 3D stress mapping by Raman, and pressure-related simulation models are highlighted to deepen the fundamental understanding of stress in ASSBs. Finally, effective strategies to reduce operating pressure are discussed, and classified into material design and cell design.

While progress has been made in reducing the pressure required for ASSBs, further advancements are needed. The following potential directions and prospects for designing low-stack-pressure ASSBs are summarized in **Figure 8**:

- Develop zero-strain active materials: Mechano-electrochemical failure can be effectively mitigated with zero-strain materials, such as $\text{Li}_4\text{Ti}_5\text{O}_{12}$,^[121] CdNb_2O_6 ,^[122] $\text{Li}_{1.75}\text{Ti}_2(\text{Ge}_{0.25}\text{P}_{0.75}\text{S}_{3.8}\text{Se}_{0.2})_3$,^[123] and high-entropy mate-

rials ($\text{LiNi}_{0.8}\text{Mn}_{0.13}\text{Ti}_{0.02}\text{Mg}_{0.02}\text{Nb}_{0.01}\text{Mo}_{0.02}\text{O}_2$).^[124] These materials exhibit minimal volume changes during cycling, reducing the risk of mechanical failure.

- Synthesize novel SSEs with good elasticity: Elastic solid-state electrolytes are more adaptable, forming intimate solid–solid contact under pressure and accommodating the volume changes of electrode materials during cycling. This flexibility enhances their performance under lower operating pressures.
- Incorporate crack-resistant materials: Integrating crack-resistant materials into electrodes helps counteract strain, maintaining stable interfacial contact and reducing the need for high operating pressures.
- Design porous materials: Porous structures can accommodate volume changes by providing space for lithium metal penetration, minimizing stress fluctuations during cycling.
- Develop integrated electrodes: Integrated electrodes without SSEs can ensure uniform expansion and contraction of the cathode during cycling, thereby mitigating the loss of electrode/SE contact.
- Control the electrochemical reaction process: Materials such as Ni-rich NCM tend to undergo significant volume changes at high states of lithiation. Adjusting the electrochemical reaction process, such as modifying the cut-off voltage, can help manage these volume changes.
- Optimize the N/P ratio: Fine-tuning the N/P ratio ensures that the contraction of the cathode is balanced by the expansion of the anode during charging, minimizing stress and strain during cycling.
- Implement constant pressure systems: Spring-loaded, quasi-constant pressure setups can help manage pressure fluctuations, mitigating the effects of volume changes during cycling.

Overall, overcoming the pressure-related challenges of ASSBs requires interdisciplinary approaches that combine innovations in material science and cell design. The proposed strategies aim to enhance the mechanical robustness and overall performance of ASSBs, while minimizing issues associated with volume changes during cycling.

Acknowledgements

J.Z. and J.F. contributed equally to this work. This work was supported by the National Natural Science Foundation of China (Grant Nos. W2441017; 22409103), the “Innovation Yongjiang 2035” Key R&D Programme (Grant No.2024Z040), the Postdoctoral Innovation Talent Support Program (Grant No. BX20240175), and the China Postdoctoral Science Foundation (Grant No. 2024M751549, 2024M751548, 2024T170442).

Conflict of Interest

The authors declare no conflict of interest.

Keywords

all-solid-state batteries, fabrication pressure, operation pressure, solid electrolytes

Received: September 9, 2024

Revised: October 30, 2024

Published online: December 26, 2024

- [1] D. Kim, X. Hu, B. Z. Yu, Y. I. Chen, *Adv. Mater.* **2024**, *36*, 2401625.
- [2] J. Sung, J. Heo, D. H. Kim, S. Jo, Y. C. Ha, D. Kim, S. Ahn, J. W. Park, *Mater. Chem. Front.* **2024**, *8*, 1861.
- [3] N. Zhao, W. Khokhar, Z. Bi, C. Shi, X. Guo, L.-Z. Fan, C.-W. Nan, *Joule* **2019**, *3*, 1190.
- [4] C. H. Wang, J. W. Liang, Y. Zhao, M. T. Zheng, X. N. Li, X. L. Sun, *Energy Environ. Sci.* **2021**, *14*, 2577.
- [5] C. H. Wang, J. W. Liang, J. T. Kim, X. L. Sun, *Sci. Adv.* **2022**, *8*, eadc9516.
- [6] P. Lennartz, B. A. Paren, A. Herzog-Arbeitman, X. C. Chen, J. A. Johnson, M. Winter, Y. Shao-Horn, G. Brunklaus, *Joule* **2023**, *7*, 1471.
- [7] L. Hu, J. Z. Wang, K. Wang, Z. Q. Gu, Z. W. Xi, H. Li, F. Chen, Y. X. Wang, Z. Y. Li, C. Ma, *Nat. Commun.* **2023**, *14*, 3807.
- [8] K. Tuo, C. W. Sun, S. Q. Liu, *Electrochem. Energy Rev.* **2023**, *6*, 17.
- [9] M. Qin, Z. Zeng, Q. Wu, H. Yan, M. Liu, Y. Wu, H. Zhang, S. Lei, S. Cheng, J. Xie, *Energy Environ. Sci.* **2023**, *16*, 546.
- [10] Y. X. Li, S. B. Song, H. Kim, K. Nomoto, H. Kim, X. Y. Sun, S. Hori, K. Suzuki, N. Matsui, M. Hirayama, T. Mizoguchi, T. Saito, T. Kamiyama, R. Kanno, *Science* **2023**, *381*, 50.
- [11] H. F. Xu, S. B. Yang, B. Li, *Adv. Energy Mater.* **2024**, *14*, 2303539.
- [12] J. Oh, W. J. Chung, S. H. Jung, Y. Kim, Y. K. Lee, Y. J. Nam, S. H. Lee, C. H. Kim, J. W. Choi, *Energy Storage Mater.* **2024**, *71*, 103606.
- [13] S. Puls, E. Nazmutdinova, F. Kalyk, H. M. Woolley, J. F. Thomsen, Z. Cheng, A. Fauchier-Magnan, A. Gautam, M. Gockeln, S.-Y. Ham, M. T. Hasan, M.-G. Jeong, D. Hiraoka, J. S. Kim, T. Kutsch, B. Lelotte, P. Minnmann, V. Miß, K. Motohashi, D. L. Nelson, F. Ooms, F. Piccolo, C. Plank, M. Rosner, S. E. Sandoval, E. Schlautmann, R. Schuster, D. Spencer-Jolly, Y. Sun, B. S. Vishnugopi, et al., *Nat. Energy* **2024**, *9*, 1310.
- [14] F. Zhang, Y. Guo, L. Zhang, P. Jia, X. Liu, P. Qiu, H. Zhang, J. Huang, *eTransportation* **2023**, *15*, 100220.
- [15] H. J. Shin, J. T. Kim, A. Y. Kim, N. Noh, J. Park, C. R. Park, S. H. Yu, H. Kim, K. Y. Chung, J. M. Yuk, S. T. Myung, H. G. Jung, *Adv. Energy Mater.* **2023**, *13*, 2301220.
- [16] X. Hu, Z. J. Zhang, X. Zhang, Y. Wang, X. Yang, X. Wang, M. Fayena-Greenstein, H. A. Yehezkel, S. Langford, D. Zhou, B. H. Li, G. X. Wang, D. Aurbach, *Nat. Rev. Mater.* **2024**, *9*, 305.
- [17] T. Dai, S. Y. Wu, Y. X. Lu, Y. Yang, Y. Liu, C. Chang, X. H. Rong, R. J. Xiao, J. M. Zhao, Y. H. Liu, W. H. Wang, L. Q. Chen, Y. S. Hu, *Nat. Energy* **2023**, *8*, 1221.
- [18] D. X. Cao, T. T. Ji, Z. X. Wei, W. T. Liang, R. B. Bai, K. S. Burch, M. Geiwitz, H. L. Zhu, *Nano Lett.* **2023**, *23*, 9392.
- [19] S.-Y. Ham, H. Yang, O. Nunez-cuacuas, D. H. S. Tan, Y.-T. Chen, G. Deysher, A. Cronk, P. Ridley, J.-M. Doux, E. A. Wu, J. Jang, Y. S. Meng, *Energy Storage Mater.* **2023**, *55*, 455.
- [20] X. W. Gao, B. Y. Liu, B. K. Hu, Z. Y. Ning, D. S. Jolly, S. M. Zhang, J. Perera, J. F. Bu, J. L. Liu, C. Doerrer, E. Darnbrough, D. Armstrong, P. S. Grant, P. G. Bruce, *Joule* **2022**, *6*, 636.
- [21] S. Y. Yin, W. T. Deng, J. Chen, X. Gao, G. Q. Zou, H. S. Hou, X. B. Ji, *Nano Energy* **2021**, *83*, 105854.
- [22] Z. L. Xu, Y. Gang, M. A. Garakani, S. Abouali, J. Q. Huang, J. K. Kim, *J. Mater. Chem. A* **2016**, *4*, 6098.
- [23] C. Reynaud, F. Sommer, C. Quet, N. El Bounia, T. M. Duc, *Surf. Interface Anal.* **2000**, *30*, 185.
- [24] G. L. Gregory, H. Gao, B. Liu, X. Gao, G. J. Rees, M. Pasta, P. G. Bruce, C. K. Williams, *J. Am. Chem. Soc.* **2022**, *144*, 17477.
- [25] S. Ramesh, T. Winie, A. K. Arof, *Eur. Polym. J.* **2007**, *43*, 1963.
- [26] S. Ramesh, T. Winie, A. K. Arof, *J. Mater. Sci.* **2010**, *45*, 1280.
- [27] Y. Chen-Yang, *Solid State Ionics* **2002**, *150*, 327.
- [28] F. P. McGrogan, T. Swamy, S. R. Bishop, E. Eggleton, L. Porz, X. Chen, Y. M. Chiang, K. J. Van Vliet, *Adv. Energy Mater.* **2017**, *7*, 1602011.
- [29] A. Kato, M. Nagao, A. Sakuda, A. Hayashi, M. Tatsumisago, *J. Ceram. Soc. Jpn.* **2014**, *122*, 552.
- [30] A. Kato, M. Nose, M. Yamamoto, A. Sakuda, A. Hayashi, M. Tatsumisago, *J. Ceram. Soc. Jpn.* **2018**, *126*, 719.
- [31] Z. Q. Wang, M. S. Wu, G. Liu, X. L. Lei, B. Xu, C. Y. Ouyang, *Int. J. Electrochem. Sc.* **2014**, *9*, 562.
- [32] Z. Deng, Z. B. Wang, I. H. Chu, J. Luo, S. P. Ong, *J. Electrochem. Soc.* **2016**, *163*, A67.
- [33] S. Smith, T. Thompson, J. Sakamoto, J. L. Allen, D. R. Baker, J. Wolfenstine, *Solid State Ionics* **2017**, *300*, 38.
- [34] S. D. Jackman, R. A. Cutler, *J. Power Sources* **2012**, *218*, 65.
- [35] A.-N. Wang, J. F. Nonemacher, G. Yan, M. Finsterbusch, J. Malzbender, M. Krüger, *J. Eur. Ceram. Soc.* **2018**, *38*, 3201.
- [36] Y. Kim, H. Jo, J. L. Allen, H. Choe, J. Wolfenstine, J. Sakamoto, *J. Am. Ceram. Soc.* **2016**, *99*, 1367.
- [37] Y.-H. Cho, J. Wolfenstine, E. Rangasamy, H. Kim, H. Choe, J. Sakamoto, *J. Mater. Sci.* **2012**, *47*, 5970.
- [38] C. Campbell, Y. M. Lee, K. Y. Cho, Y. G. Lee, B. Lee, C. Phatak, S. Hong, *Sci. Rep.* **2018**, *8*, 2514.
- [39] J. H. Hu, Z. T. Sun, Y. R. Gao, P. Li, Y. F. Wu, S. W. Chen, R. B. Wang, N. A. Li, W. E. Yang, Y. X. Shen, S. H. Bo, *Cell Rep. Phys. Sci.* **2022**, *3*, 100938.
- [40] S. Monismith, J. Qu, *J. Phys. Chem. C* **2021**, *125*, 10777.
- [41] C. Schneider, C. P. Schmidt, A. Neumann, M. Clausnitzer, M. Sadowski, S. Harm, C. Meier, T. Danner, K. Albe, A. Latz, W. A. Wall, B. V. Lotsch, *Adv. Energy Mater.* **2023**, *13*, 2203837.
- [42] B. Rieger, S. Schlueter, S. V. Erhard, A. Jossena, *J. Electrochem. Soc.* **2016**, *163*, A1595.
- [43] W. Zhao, Y. Zhang, N. Sun, Q. S. Liu, H. W. An, Y. J. Song, B. Deng, J. Wang, G. P. Yin, F. P. Kong, S. F. Lou, J. J. Wang, *ACS Energy Lett.* **2023**, *8*, 5050.

- [44] H. K. Tian, A. Chakraborty, A. A. Talin, P. Eisenlohr, Y. Qi, *J. Electrochem. Soc.* **2020**, *167*, 090541.
- [45] H. W. Gao, X. Ai, H. C. Wang, W. Q. Li, P. Wei, Y. Cheng, S. W. Gui, H. Yang, Y. Yang, M. S. Wang, *Nat. Commun.* **2022**, *13*, 5050.
- [46] J. B. Gu, X. X. Chen, Z. F. He, Z. T. Liang, Y. Lin, J. W. Shi, Y. Yang, *Adv. Energy Mater.* **2023**, *13*, 2302643.
- [47] K. Funayama, T. Nakamura, N. Kuwata, J. Kawamura, T. Kawada, K. Amezawa, *Electrochem.* **2015**, *83*, 894.
- [48] E. J. Fuller, D. S. Ashby, C. Polop, E. Salagre, B. Bhargava, Y. Song, E. Vasco, J. D. Sugar, P. Albertus, T. O. Menteş, A. Locatelli, P. Segovia, M. Á. Gonzalez-Barrio, A. Mascaraque, E. G. Michel, A. A. Talin, *ACS Nano* **2022**, *16*, 16363.
- [49] J. Sang, B. Tang, Y. Qiu, Y. Fang, K. Pan, Z. Zhou, *Energy Environ. Mater.* **2023**, *7*, e12670.
- [50] M. Cronau, M. Szabo, C. König, T. B. Wassermann, B. Roling, *ACS Energy Lett.* **2021**, *6*, 3072.
- [51] X. S. Liu, B. Z. Zheng, J. Zhao, W. M. Zhao, Z. T. Liang, Y. Su, C. P. Xie, K. Zhou, Y. X. Xiang, J. P. Zhu, H. C. Wang, G. M. Zhong, Z. L. Gong, J. Y. Huang, Y. Yang, *Adv. Energy Mater.* **2021**, *11*, 2003583.
- [52] J. Y. Wang, L. Liao, Y. Z. Li, J. Zhao, F. F. Shi, K. Yan, A. L. Pei, G. X. Chen, G. D. Li, Z. Y. Lu, Y. Cui, *Nano Lett.* **2018**, *18*, 7060.
- [53] Y. Qi, C. M. Ban, S. J. Harris, *Joule* **2020**, *4*, 2599.
- [54] J. M. Doux, Y. Y. C. Yang, D. H. S. Tan, H. Nguyen, E. A. Wu, X. F. Wang, A. Banerjee, Y. S. Meng, *J. Mater. Chem. A* **2020**, *8*, 5049.
- [55] C. R. Fell, D. H. Lee, Y. S. Meng, J. M. Gallardo-Amores, E. Moran, M. E. Arroyo-de Domípablo, *Energy Environ. Sci.* **2012**, *5*, 6214.
- [56] J. Park, J. Jeong, Y. Lee, M. Oh, M. H. Ryou, Y. M. Lee, *Adv. Mater. Interfaces* **2016**, *3*, 1600140.
- [57] R. Koerver, I. Aygün, T. Leichtweiss, C. Dietrich, W. B. Zhang, J. O. Binder, P. Hartmann, W. G. Zeier, J. Janek, *Chem. Mater.* **2017**, *29*, 5574.
- [58] R. Koerver, W. B. Zhang, L. de Biasi, S. Schweidler, A. O. Kondrakov, S. Kolling, T. Brezesinski, P. Hartmann, W. G. Zeier, J. Janek, *Energy Environ. Sci.* **2018**, *11*, 2142.
- [59] S. Jun, Y. J. Nam, H. Kwak, K. T. Kim, D. Y. Oh, Y. S. Jung, *Adv. Funct. Mater.* **2020**, *30*, 2002535.
- [60] S.-K. Jung, H. Gwon, G. Yoon, L. J. Miara, V. Lacivita, J.-S. Kim, *ACS Energy Lett.* **2021**, *6*, 2006.
- [61] G. V. Alexander, C. M. Shi, J. O'Neill, E. D. Wachsman, *Nat. Mater.* **2023**, *22*, 1136.
- [62] M. J. Lee, J. Han, K. Lee, Y. J. Lee, B. G. Kim, K.-N. Jung, B. J. Kim, S. W. Lee, *Nature* **2022**, *601*, 217.
- [63] D. Y. Oh, Y. J. Nam, K. H. Park, S. H. Jung, K. T. Kim, A. R. Ha, Y. S. Jung, *Adv. Energy Mater.* **2019**, *9*, 1802927.
- [64] Y. Han, S. H. Jung, H. Kwak, S. Jun, H. H. Kwak, J. H. Lee, S. T. Hong, Y. S. Jung, *Adv. Energy Mater.* **2021**, *11*, 2100126.
- [65] C. H. Wang, R. Z. Yu, S. Hwang, J. W. Liang, X. N. Li, C. T. Zhao, Y. P. Sun, J. W. Wang, N. Holmes, R. Y. Li, H. Huang, S. Q. Zhao, L. Zhang, S. G. Lu, D. Su, X. L. Sun, *Energy Storage Mater.* **2020**, *30*, 98.
- [66] C. Doerrer, I. Capone, S. Narayanan, J. L. Liu, C. R. M. Grovenor, M. Pasta, P. S. Grant, *ACS Appl. Mater. Interfaces* **2021**, *13*, 37809.
- [67] R. Gao, M. Zhang, Z. Han, X. Xiao, X. Wu, Z. Piao, Z. Lao, L. Nie, S. Wang, G. Zhou, *Adv. Mater.* **2023**, *36*, 2303610.
- [68] S. C. Jo, J. W. Hong, I. H. Choi, M. J. Kim, B. G. Kim, Y. J. Lee, H. Y. Choi, D. Kim, T. Kim, K. J. Baeg, J. W. Park, *Small* **2022**, *18*, 2200326.
- [69] J. U. Lee, C. Zhao, C. H. Wang, A. N. Chen, X. L. Sun, K. Amine, G. L. Xu, *Chem. Soc. Rev.* **2024**, *53*, 5264.
- [70] J. B. Zhou, M. L. H. Chandrappa, S. Tan, S. Wang, C. S. Wu, H. Nguyen, C. H. Wang, H. D. Liu, S. C. Yu, Q. R. S. Miller, G. Hyun, J. Holoubek, J. H. Hong, Y. X. Xiao, C. Soulen, Z. Fan, E. E. Fullerton, C. J. Brooks, C. Wang, R. J. Clément, Y. Yao, E. Y. Hu, S. P. Ong, P. Liu, *Nature* **2024**, *627*, 301.
- [71] M. J. Si, X. F. Jian, Y. Xie, J. H. Zhou, W. Jian, J. Lin, Y. F. Luo, J. Y. Hu, Y. J. Wang, D. Zhang, T. F. Wang, Y. J. Liu, Z. L. Wu, S. Y. Zheng, J. T. Yang, *Adv. Energy Mater.* **2024**, *14*, 2303991.
- [72] J.-H. Bae, S.-R. Lee, H.-Y. Choi, J.-W. Park, B. G. Kim, D. Kim, S.-Y. Yoon, Y.-J. Lee, *Appl. Surf. Sci.* **2023**, *614*, 156112.
- [73] R. Q. Ma, Y. T. Fan, Y. T. Jin, S. Y. Pan, H. Y. Zhong, Y. Luo, J. B. Gu, M. Z. Luo, Y. Q. Wu, W. X. Hu, P. Z. Chen, Y. Su, G. Y. Wu, J. W. Yan, J. Gao, Z. L. Gong, Y. Yang, *Adv. Energy Mater.* **2024**, *14*, 2304412.
- [74] H. F. Xu, Q. Zhu, Y. Zhao, Z. G. Du, B. Li, S. B. Yang, *Adv. Mater.* **2023**, *35*, 2212111.
- [75] B. Hennequart, M. Platonova, R. Chometon, T. Marchandier, A. Benedetto, E. Quemin, R. Dugas, C. Lethien, J. M. Tarascon, *ACS Energy Lett.* **2024**, *9*, 454.
- [76] X. Zhang, C. Q. Luo, N. Menga, H. Zhang, Y. X. Li, S. P. Zhu, *Cell Rep. Phys. Sci.* **2023**, *4*, 101328.
- [77] J. Han, M. J. Lee, K. Lee, Y. J. Lee, S. H. Kwon, J. H. Min, E. Lee, W. Lee, S. W. Lee, B. J. Kim, *Adv. Mater.* **2023**, *35*, 2205194.
- [78] T. Y. Kwon, K. T. Kim, D. Y. Oh, Y. B. Song, S. Jun, Y. S. Jung, *Energy Storage Mater.* **2022**, *49*, 219.
- [79] W. Cho, J. Park, K. Kim, J. S. Yu, G. Jeong, *Small* **2021**, *17*, 1902138.
- [80] Z. Ning, D. S. Jolly, G. Li, R. De Meyere, S. D. Pu, Y. Chen, J. Kasemchainan, J. Ihli, C. Gong, B. Liu, *Nat. Mater.* **2021**, *20*, 1121.
- [81] J. A. Lewis, F. J. Q. Cortes, Y. Liu, J. C. Miers, A. Verma, B. S. Vishnugopoli, J. Tippens, D. Prakash, T. S. Marchese, S. Y. Han, *Nat. Mater.* **2021**, *20*, 503.
- [82] M. Peng, K. Shin, L. Jiang, Y. Jin, K. Zeng, X. Zhou, Y. Tang, *Angew. Chem.* **2022**, *134*, 202206770.
- [83] D. Cheng, T. Wynn, B. Lu, M. Marple, B. Han, R. Shimizu, B. Sreenarayanan, J. Bickel, P. Hosemann, Y. Yang, *Nat. Nanotech.* **2023**, *18*, 1448.
- [84] H. Gao, X. Ai, H. Wang, W. Li, P. Wei, Y. Cheng, S. Gui, H. Yang, Y. Yang, M.-S. Wang, *Nat. Commun.* **2022**, *13*, 5050.
- [85] J. M. Doux, H. Nguyen, D. H. S. Tan, A. Banerjee, X. F. Wang, E. A. Wu, C. Jo, H. D. Yang, Y. S. Meng, *Adv. Energy Mater.* **2020**, *10*, 1903253.
- [86] Z. Y. Ning, G. C. Li, D. L. R. Melvin, Y. Chen, J. F. Bu, D. Spencer-Jolly, J. L. Liu, B. K. Hu, X. W. Gao, J. Perera, C. Gong, S. D. D. Pu, S. M. Zhang, B. Y. Liu, G. O. Hartley, A. J. Bodey, R. I. Todd, P. S. Grant, D. E. J. Armstrong, T. J. Marrow, C. W. Monroe, P. G. Bruce, *Nature* **2023**, *618*, 287.
- [87] H. Wan, Z. Wang, W. Zhang, X. He, C. Wang, *Nature* **2023**, *623*, 739.
- [88] W. X. Ji, X. Z. Zhang, M. Liu, T. Y. Ding, H. N. Qu, D. T. Qiu, D. Zheng, D. Y. Qu, *Energy Storage Mater.* **2022**, *53*, 613.
- [89] W. B. Zhang, D. Schröder, T. Arlt, I. Manke, R. Koerver, R. Pinedo, D. A. Weber, J. Sann, W. G. Zeier, J. Janek, *J. Mater. Chem. A* **2017**, *5*, 9929.
- [90] S. Y. Han, C. Lee, J. A. Lewis, D. Yeh, Y. Liu, H. W. Lee, M. T. McDowell, *Joule* **2021**, *5*, 2450.
- [91] D. Shin, J. K. Jung, Y. Roh, C. Park, I. Kim, H. Kwon, J. Baek, W. Oh, J. Kim, S. Jeong, J. Hwang, Y. Kim, D. H. Yoon, H. T. Kim, *ACS Energy Lett.* **2024**, *9*, 1035.
- [92] X. Y. Zhang, Q. Xiang, S. Tang, A. X. Wang, X. J. Liu, J. Y. Luo, *Nano Lett.* **2020**, *20*, 2871.
- [93] S. M. Zhang, G. J. Yang, Z. P. Liu, S. T. Weng, X. Y. Li, X. F. Wang, Y. R. Gao, Z. X. Wang, L. Q. Chen, *ACS Energy Lett.* **2021**, *6*, 4118.
- [94] H. Y. Huo, J. Janek, *ACS Energy Lett.* **2022**, *7*, 4005.
- [95] Z. F. Sun, Q. Z. Yin, H. Y. Chen, M. Li, S. H. Zhou, S. F. Wen, J. H. Pan, Q. Z. Zheng, B. Jiang, H. D. Liu, K. Kim, J. Li, X. Han, Y. B. He, L. Zhang, M. C. Li, Q. B. Zhang, *Interdiscip. Mater.* **2023**, *2*, 635.
- [96] S. G. Jun, G. H. Y. Lee, Y. B. Song, H. Lim, K. H. Baeck, E. S. Lee, J. Y. Kim, D. W. Kim, J. H. Park, Y. S. Jung, *Small* **2024**, *20*, 2309437.
- [97] D. He, M. Yuan, B. Hu, C. Zou, X. Zhao, C. Zhao, J. Wang, H. Ding, *J. Phys. Conf. Ser.* **2024**, *2679*, 012005.

- [98] H. Pan, L. Wang, Y. Shi, C. Sheng, S. Yang, P. He, H. Zhou, *Nat. Commun.* **2024**, *15*, 2263.
- [99] T. Asakura, T. Inaoka, C. Hotehama, H. Kowada, K. Motohashi, A. Sakuda, M. Tatsumisago, A. Hayashi, *ACS Appl. Mater. Interfaces* **2023**, *15*, 31403.
- [100] Y.-G. Lee, S. Fujiki, C. Jung, N. Suzuki, N. Yashiro, R. Omoda, D.-S. Ko, T. Shiratsuchi, T. Sugimoto, S. Ryu, J. H. Ku, T. Watanabe, Y. Park, Y. Aihara, D. Im, I. T. Han, *Nat. Energy* **2020**, *5*, 299.
- [101] Y. S. Park, K. Kim, J. W. Lee, J. W. Moon, H. H. Park, H. Hwang, *J. Am. Ceram. Soc.* **2023**, *106*, 7322.
- [102] S. G. Yoon, B. S. Vishnugopi, E. P. Alsaç, W. J. Jeong, S. E. Sandoval, D. L. Nelson, A. Ayyaswamy, P. P. Mukherjee, M. T. McDowell, *ACS Nano* **2024**, *18*, 20792.
- [103] J. Oh, S. H. Choi, J. Y. Kim, J. Lee, T. Lee, N. Lee, T. Y. Lee, Y. Sohn, W. J. Chung, K. Y. Bae, S. Son, J. W. Choi, *Adv. Energy Mater.* **2023**, *13*, 2301508.
- [104] J. Oh, S. H. Choi, B. Chang, J. Lee, T. Lee, N. Lee, H. Kim, Y. Kim, G. Im, S. Lee, J. W. Choi, *ACS Energy Lett.* **2022**, *7*, 1374.
- [105] J. Oh, S. H. Choi, H. Kim, J. Y. Kim, G.-J. Lee, K. Y. Bae, T. Lee, N. Lee, Y. Sohn, W. J. Chung, J. W. Choi, *Energy Environ. Sci.* **2024**, *17*, 7932.
- [106] S. E. Sandoval, J. A. Lewis, B. S. Vishnugopi, D. L. Nelson, M. M. Schneider, F. J. Q. Cortes, C. M. Matthews, J. Watt, M. K. Tian, P. Shevchenko, P. P. Mukherjee, M. T. McDowell, *Joule* **2023**, *7*, 2054.
- [107] Z. T. Sun, J. Y. Zhou, Y. F. Wu, S. H. Bo, *J. Phys. Chem. Lett.* **2022**, *13*, 10816.
- [108] D. Y. Cheng, T. Wynn, B. Y. Lu, M. Marple, B. Han, R. Shimizu, B. Sreenarayanan, J. Bickel, P. Hosemann, Y. Y. C. Yang, H. Nguyen, W. K. Li, G. M. Zhu, M. H. Zhang, Y. S. Meng, *Nat. Nanotech.* **2023**, *18*, 1448.
- [109] Y. M. Song, B. Bhargava, D. M. Stewart, A. A. Talin, G. W. Rubloff, P. Albertus, *Joule* **2023**, *7*, 652.
- [110] M. Yamamoto, Y. Terauchi, A. Sakuda, A. Kato, M. Takahashi, *J. Power Sources* **2020**, *473*, 228595.
- [111] H. D. Yang, Z. J. Wang, *J. Solid State Electrochem.* **2023**, *27*, 2607.
- [112] B. Y. Liu, S. D. Pu, C. Doerrer, D. Spencer Jolly, R. A. House, D. L. R. Melvin, P. Adamson, P. S. Grant, X. W. Gao, P. G. Bruce, *Susmat* **2023**, *3*, 721.
- [113] J. B. Gu, Z. T. Liang, J. W. Shi, Y. Yang, *Adv. Energy Mater.* **2023**, *13*, 2203153.
- [114] J. Peng, D. Wu, P. Lu, Z. Wang, Y. Du, Y. Wu, Y. Wu, W. Yan, J. Wang, H. Li, L. Chen, F. Wu, *Energy Storage Mater.* **2023**, *54*, 430.
- [115] B. Hennequart, M. Deschamps, R. Chometon, B. Leube, R. Dugas, E. Quemin, P.-E. Cabelguen, C. Lethien, J.-M. Tarascon, *ACS Appl. Energy Mater.* **2023**, *6*, 8521.
- [116] Y. X. Ren, W. Shin, A. Manthiram, *Adv. Energy Mater.* **2022**, *12*, 2200190.
- [117] T. Fuchs, C. G. Haslam, A. C. Moy, C. Lerch, T. Krauskopf, J. Sakamoto, F. H. Richter, J. Janek, *Adv. Energy Mater.* **2022**, *12*, 2201125.
- [118] Y.-T. Chen, J. Jang, J. A. S. Oh, S.-Y. Ham, H. Yang, D.-J. Lee, M. Vicencio, J. B. Lee, D. H. Tan, M. Chouchane, *Adv. Energy Mater.* **2024**, *14*, 2304327.
- [119] C. Lee, J. Y. Kim, K. Y. Bae, T. Kim, S. J. Jung, S. Son, H. W. Lee, *Energy Storage Mater.* **2024**, *66*, 103196.
- [120] Y. Sakka, H. Yamashige, A. Watanabe, A. Takeuchi, M. Uesugi, K. Uesugi, Y. Orikasa, *J. Mater. Chem. A* **2022**, *10*, 16602.
- [121] Z. Q. Zhang, S. Y. Lu, G. Huang, W. J. Wang, D. C. He, Y. Liu, F. Gao, Y. H. Chen, H. R. Zhan, J. Mei, M. Terrones, Y. Q. Wang, X. C. Chen, *Carbon* **2024**, *221*, 118855.
- [122] C. Cheng, D. Wu, T. Gong, Y. Yan, Y. Liu, W. Ji, L. Hou, C. Yuan, *Adv. Energy Mater.* **2023**, *13*, 2302107.
- [123] L. F. Cui, S. Zhang, J. W. Ju, T. Liu, Y. Zheng, J. H. Xu, Y. T. Wang, J. D. Li, J. W. Zhao, J. Ma, J. Z. Wang, G. J. Xu, T. S. Chan, Y. C. Huang, S. C. Haw, J. M. Chen, Z. W. Hu, G. L. Cui, *Nat. Energy* **2024**, *9*, 1084.
- [124] R. Zhang, C. Y. Wang, P. C. Zou, R. Q. Lin, L. Ma, L. Yin, T. Y. Li, W. Q. Xu, H. Jia, Q. Y. Li, S. Sainio, K. Kisslinger, S. E. Trask, S. N. Ehrlich, Y. Yang, A. M. Kiss, M. Y. Ge, B. J. Polzin, S. J. Lee, W. Xu, Y. Ren, H. L. Xin, *Nature* **2022**, *610*, 67.



Jiaxu Zhang is currently a postdoctoral researcher under the supervision of Prof. Xueliang (Andy) Sun at the Eastern Institute for Advanced Study (EIAS) and the University of Science and Technology of China (USTC). He received his B.S. at Wuhan University of Technology (WHUT) in 2018. He completed his Ph.D. at the Wuhan University of Technology in 2023, studying material science and technology. His research interests mainly focus on low-pressure all-solid-state batteries.



Jiamin Fu received his B.S. in New Energy Materials and Devices from Central South University in 2016. He completed his M.S. at the University of Chinese Academy of Sciences in 2019 and Ph.D. at the University of Western Ontario in 2023, studying material physics and chemistry. His Ph. D. studies focused on the development of all-solid-state batteries and synchrotron-related characterization techniques. Dr. Fu is currently a postdoctoral fellow in Mechanical and Materials Engineering at the University of Western Ontario.



Pushun Lu is currently a postdoctoral researcher under the supervision of Prof. Xueliang (Andy) Sun at the Eastern Institute for Advanced Study (EIAS). He received his BS degree from Xiamen University in 2018 and Ph.D. degree from the University of Chinese Academy of Sciences in 2023. His research interests mainly focus on solid electrolyte materials and low-temperature all-solid-state batteries.



Guantai Hu received his Ph.D. degree in materials science and engineering at Iowa State University. He is now a postdoctoral researcher at the Eastern Institute of Technology, Ningbo. His research interests are focused on advanced materials for all-solid-state batteries.



Shengjie Xia received his M.S. at the University of Science and Technology of China in 2022, studying material engineering. He is currently a doctoral student in the School of Chemistry and Chemical Engineering at Shanghai Jiao Tong University, studying materials and chemical industry.



Shutao Zhang received his bachelor's degree in Materials Chemistry in 2019 from the China University of Petroleum (East China) and a Master's Degree in Materials Engineering in 2022 from the University of Chinese Academy of Sciences. He is currently a doctoral student in the School of Chemistry and Chemical Engineering in Shanghai Jiao Tong University, studying materials and chemical industry.



Ziqing Wang received her bachelor's degree in Applied Chemistry in 2020 from Anhui Agricultural University and her Master's Degree in Chemistry in 2023 from the School of Materials Science and Engineering, Huaqiao University. She is currently a doctor in Prof. Xueliang Sun's group at the University of Science and Technology of China. Her research interest concentrates on advanced cathode materials and solid-state electrolytes for high-performance lithium-ion batteries and solid-state batteries.



Zhimin Zhou is currently a PhD in Prof. Changhong Wang's Group at the Eastern Institute of Technology, Ningbo, China. He got his BS in chemical engineering and technology from the University of Northwestern Polytechnical University in 2018 and obtained his MS degree in chemical engineering from the University of Chinese Academy of Sciences in 2021. After graduation, he also served as an algorithm engineer at the company from 2021 to 2023. Currently, his research interests focus on the synthesis of halide solid electrolytes as well as all-solid-state lithium batteries.



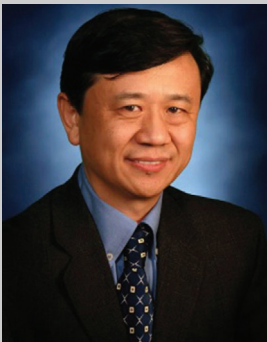
Wenlin Yan received her master's degree from the Institute of Physics, Chinese Academy of Science in 2022. She is currently a PhD student at the University of California, San Diego, under the supervisor of Prof. Ping Liu, studying batteries recycling and all solid-state batteries.



Wei Xia is an Assistant Professor in the College of Science at the Eastern Institute of Technology, Ningbo. He obtained his Ph.D. degree in 2016 from Peking University under the guidance of Prof. Ruqiang Zou. Following this, he completed postdoctoral research at the University of Western Ontario with Prof. Xueliang Sun and served as an Associate Research Fellow at the Southern University of Science and Technology with Prof. Yusheng Zhao. His research centers on advanced neutron diffraction techniques and innovations in all-solid-state batteries.



Changhong Wang is currently an Assistant Professor at the Eastern Institute for Advanced Study (EIAS), Eastern Institute of Technology (Tentative), Ningbo since 2023. He received his M.S. degree in Material Engineering from the University of Science and Technology of China in 2014 and his Ph.D. degree in Mechanical and Material Engineering from the University of Western Ontario (UWO) in 2020. Before joining EIAS, He was a Banting Postdoctoral Fellow at the University of Maryland at College Park and a Visiting Researcher at UWO. His research interests focus on key materials and key technologies for all-solid-state batteries.



Xueliang Sun is currently a Chair Professor at the Eastern Institute of Technology, Ningbo. His research interests include all-solid-state batteries, lithium-ion batteries, and fuel cells. Dr. Xueliang Sun is an author of over 630 refereed journals (e.g. *Nature Energy*, *Nature Communications*, *Science Advances*) with citations of over 60 000 times and an H-index of 128. Dr. Sun received various awards such as the Award for Research Excellence in Materials Chemistry Winner from the Canada Chemistry Society and the IBA Battery Technology Award. He has been selected as a "Global Highly Cited Scientist" and "World Top 2% Top Scientists" by Clarivate Analytics since.